

POLITECNICO DI TORINO

DIMEAS - DEPARTMENT OF MECHANICAL AND AEROSPACE
ENGINEERING

MASTER OF SCIENCE DEGREE
IN
AUTOMOTIVE ENGINEERING

Master's degree thesis

**Lateral and longitudinal control of
an autonomous racing vehicle**



Supervisors:

Prof. Nicola Amati
Prof. Angelo Bonfitto

Candidate:

Kiran Kone
239599

Academic Year 2018-2019

Abstract

The development of autonomous and intelligent vehicles is increasing continuously in the aim to reach a reliable and secured transportation system. Indeed, autonomous navigation include three main steps: perception and localization, planning and control.

This thesis covers essentially the study of the vehicle modeling and the vehicle control, focused on the coupled lateral and longitudinal control of the autonomous racing vehicle. Three different control strategies are considered: First one based on coupled control while the second one is decoupled control. In coupled controller, adaptive model predictive control (MPC) is used which handles both lateral and longitudinal control. In the decoupled control strategy, longitudinal dynamics is controlled with the help of a PID and Lateral dynamics is controlled first with MPC and second with Lateral controller.

The proposed strategy utilizes an adaptive MPC to perform lateral guidance and speed regulation by acting on the front wheel steering angle and acceleration/deceleration to minimize the vehicle's lateral deviation and relative yaw angle with respect to the reference trajectory, while driving the vehicle within the limits of adherence conditions.

While designing the Adaptive-MPC, the internal plant model for MPC is modeled using a linear bicycle model, while dynamics of the vehicle is modeled using a 3 degree of freedom dual-track rigid vehicle model considering the non-linear tire forces derived from a Pacejka model taking into account the slip ratio.

The objective is to develop and analyse the three different control strategies and evaluate their design and performance through path following, speed tracking, and ease of implementation. The overall system has been developed using MATLAB® and Simulink®.

Acknowledgements

I would like to extend my sincere gratitude towards my thesis supervisor, Prof. Nicola Amati for providing with this opportunity. I am extremely grateful to Dr. Angelo Bonfitto for valuable feedback and constructive suggestions for this master thesis.

I would like to offer my special thanks to Shailesh Hegde, for his guidance and valuable suggestion for this thesis.

I would like to thank Irfan Khan for his continuous support and valuable advice for this thesis.

Finally, but not least, I would like to express my profound gratitude to my family and friends for providing me with unfailing support and continuous encouragement throughout my years of study.

Contents

List of Figures	III
1 Introduction	1
1.1 Thesis motivation	1
1.2 Driving at the Handling Limits	3
1.2.1 Exceeding the Friction Limits: Understeer and Oversteer	4
1.3 State of the art	6
1.4 Thesis outline	9
2 Modelling	10
2.1 Vehicle model for validation and simulation	11
2.1.1 Kinematic model	11
2.1.2 Dynamic model	15
2.2 Tire models	18
2.2.1 Pacejka tire model	21
2.2.2 Logitudinal Tire Forces	22
2.2.3 Lateral Tire Forces	23
2.3 Vehicle model for MPC	26
2.4 Driveline dynamics	30
3 Control design	33
3.1 Lane detection	35
3.2 Reference trajectory generation	36
3.2.1 Trajectory curvature computation	37
3.2.2 Computation of vehicle model dynamic parameters	40
3.3 Reference speed profile generation	41

3.4	Model Predictive Control	44
3.4.1	Overview of MPC	44
3.4.2	MPC problem formulation	48
3.5	Decoupled Controller	54
3.5.1	PID Controller	56
3.5.2	Stanley Controller	57
4	Results and discussions	59
4.1	Setup	59
4.1.1	Racetrack and The Car	59
4.2	Results and discussion	61
4.2.1	Sensitivity Analysis of MPC	61
4.2.2	Weights and Constraints	62
4.2.3	Coupled Controller: MPC	64
4.2.4	Comparison with decoupled controller: MPC+PID and PID+P	67
4.3	Validation of Controller	71
4.3.1	Acceleration Test	71
4.3.2	Skid Pad Test	72
5	Conclusions and future works	75
	Bibliography	77

List of Figures

1.1	Friction circle	4
1.2	(a) Vehicle understeering at the limits of handling. (b) Vehicle oversteering at the limits of handling	5
1.3	Global architecture of control strategy for autonomous driving presented in this thesis	8
2.1	Vehicle kinematic model	12
2.2	Model Coordinate Systems	15
2.3	3 DoF rigid vehicle model	16
2.4	Classification of tire models	18
2.5	Illustration of the tire model	19
2.6	Coefficients of the Pacejka model for different road condition	22
2.7	Lateral tire force regions	24
2.8	Tire slip angle	25
2.9	Bicycle model in terms of lateral deviation and relative yaw angle with respect to the center line of the lane	27
2.10	Driveline dynamics architecture	31
2.11	Lower dynamics architecture	32
3.1	Detailed architecture of the control strategy	34
3.2	Sensor Simulation	35
3.3	Curve α and tangential angle ϕ	38
3.4	Demonstration that the definition 3.1 can be derived from the definition 3.2	38
3.5	Osculating circle and radius of curvature	39

3.6	Definition of lateral deviation and relative yaw angle with respect the center line of the lane	41
3.7	Center line, curvature, lateral deviation and relative yaw angle com- putation	41
3.8	Block diagram for Model Predictive Control	45
3.9	Basic concept for Model Predictive Control	47
3.10	Architecture of MPC Controller	53
3.11	Architecture of MPC-PID controller	55
3.12	Architecture of PID-Stanley controller	55
3.13	PID feedback loop	56
3.14	Stanley controller	57
4.1	(a)Racetrack scenario (b) Detected road curvature k	60
4.2	Basic workflow for designing traditional model predictive controllers	61
4.3	MPC Constraints and Weights	63
4.4	Measured vehicle's longitudinal speed V_x (dashed) vs. vehicle's lon- gitudinal speed reference V_{ref} (solid)	64
4.5	Lateral deviation e_1	65
4.6	Relative yaw angle e_2	65
4.7	Front wheels steering angle command δ	66
4.8	GG plot with the ellipse representing the adherence limits-MPC . .	66
4.9	Measured vehicle's longitudinal speed V_x (dashed) vs. vehicle's lon- gitudinal speed reference V_{ref} (solid)	67
4.10	Lateral deviation e_1	68
4.11	Relative yaw angle e_2	68
4.12	Front wheels steering angle command δ	69
4.13	GG plot with the ellipse representing the adherence limits MPC . .	70
4.14	GG plot with the ellipse representing the adherence limits (A)MPC+PID (B)PID+P	70
4.15	Acceleration Test Track	71
4.16	Acceleration Test Data	72
4.17	Logitudinal veocity	72
4.18	Skid-Pad Test Track	73
4.19	Skid-Pad Test Data	73

4.20 Skidpad MPC 74
4.21 Skidpad (A)MPC+PID (B) PID+P 74

Chapter 1

Introduction

1.1 Thesis motivation

The traffic in the world and the number of cars is rapidly increasing. At present, there are roughly a 1.2 billion cars in the world. Yet within twenty years, the number will double to 2 billion [1]. Every year the lives of approximately 1.35 million people are cut short as a result of a road traffic crash. Between 20 and 50 million more people suffer non-fatal injuries, with many incurring a disability as a result of their injury [2]. Transport is responsible for nearly 30% of the EU's total CO₂ emissions, of which 72% comes from road transportation. As part of efforts to reduce CO₂ emissions, the EU has set a goal of reducing emissions from transport by 60% by 2050 compared to 1990 levels. This all has led to new challenges such as passenger safety and comfort, fuel consumption optimization and the reduction of pollutant emissions.

Autonomous cars can help to reduce these problems, as they can achieve better traffic flow and to be more efficient, this gives a high potential to reduce fuel consumption and emissions caused by traffic and reduce the risk of accidents among other benefits. Autonomous control is an important new subfield in the automotive sector as commercial autopilots and driver assistance systems become more and more popular. While a large portion of autonomous vehicle research and development is focused on handling routine driving situations, achieving the safety benefits of autonomous vehicles also requires a focus on automated driving at the

limits of tire friction. The need for an automated vehicle to fully utilize its capability can arise when avoiding a collision with human-operated vehicles. This is crucial from an automotive safety standpoint as human error accounts for over 90 of automobile accidents [3], and there will likely be a significant period of time where autonomous vehicles must interact with human-operated vehicles [4]. Furthermore, successful handling at the friction limits will be required where environmental factors are involved, such as unpredicted natural obstructions and poor tire friction caused by inclement weather (e.g. ice, rain). The potential for technology to assist in friction-limited situations has already been demonstrated by electronic stability control (ESC) systems, which reduced single-vehicle accidents by 36% in 2007 [5] and are now standard on all passenger cars.

Autonomous racing is an emerging field within autonomous driving. In the last years, a few self-racing vehicles have been developed, both in academic and in the industrial research. The first known autonomous vehicle competition was the DARPA Grand Challenge, [6] which motivated the development of several autonomous cars in a two-year period. These cars had to compete in a desert environment and drive through a way-point corridor given shortly before the race. In this sense, it is like FSD since a short period for mapping is allowed just before the race. They however differ in that the FSD track is asphalt, the vehicles are designed for racing and reached over 90km/h and 10m/s² accelerations. Other autonomous racecars were developed afterwards [7], but their main goal was vehicle dynamic control. In addition, several scaled racecars were developed [8] but they focus on control and have an external localization system. Others were developed with on-board sensors only [9] but the focus also lied on control.

Given the highly visible marketing opportunity provided by racing, several automotive companies have made notable attempts at racing-inspired automated driving. In 2008, BMW introduced the "Track Trainer", which records race data collected from a professional driver. To "replay" the professional's driving autonomously, the vehicle tracks the pre-recorded speed and racing line with a proportional-derivative controller for throttle and brake and a dynamic programming algorithm for steering [10]. Using pre-recorded inputs allows the controller to naively account for non-linear vehicle dynamics at the handling limits, although this approach limits the exibility of the controller to respond to unpredicted events.

A second German luxury brand, Audi AG, also launched a collaborative research

effort with Stanford University in 2008. The collaboration, with which this doctoral research is affiliated, resulted in the development of Shelley, an autonomous Audi TTS. Doctoral work by Stanford students Theodosis [11] and Kritayakirana [12] provided initial forays into racing line generation and trajectory-following algorithms. Notable early accomplishments include autonomous driving at speeds of 190 mph at the Salt Flats in Utah and an autonomous drive up the Pikes Peak International Hill Climb in 2009[13][14]. More recently, Audi has incorporated results from the collaboration to build a demonstration vehicle for media events, Bobby, an autonomous RS7 which debuted at Germany's Hockenheimring [15]. The primary focus for the RS7 vehicle was robustness, enabling the vehicle to be demonstrated at a public event with journalists inside the vehicle at high speeds.

Finally, Autonomous car racing is a challenging task for automatic control systems due to the need for handling the vehicle close to its stability limits and in highly nonlinear operating regimes. In addition, dynamically changing racing situations require advanced path planning mechanisms with obstacle avoidance executed in real-time. Fast dynamics constrain the sampling time to be in the range of a few tens of milliseconds at most, which severely limits the admissible computational complexity of the algorithms.

1.2 Driving at the Handling Limits

Each of the four tires on an automobile contacts the road surface over a contact patch, an area roughly the size of a human hand. As shown in Figure 1.1 these contact patches generate the friction forces between the tire and road that are necessary for both vehicle longitudinal acceleration (braking and acceleration) as well as lateral acceleration (turning). Because the available friction between the tire and road is limited, each of the four tires is limited in the turning, braking, and accelerating forces they can produce. This relationship is given for each tire by the commonly known "friction circle" equation:

$$\sqrt{F_x^2 + F_y^2} < \mu F_z \tag{1.1}$$

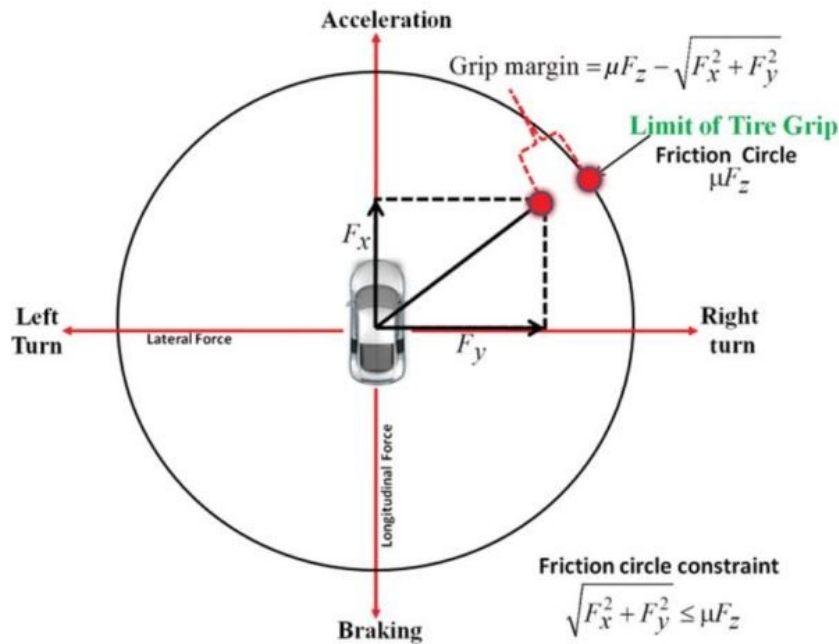


Figure 1.1: Friction circle

where μ is the friction coefficient between the tire and the road, F_z is the normal force acting on the tire, and F_y and F_x are the lateral and longitudinal forces, respectively Figure 1.1. One key insight from Figure 1.1 is that the cornering and braking ability of the car is heavily determined by the amount of friction. On a dry, paved asphalt surface, values of μ are typically equal to 1.0. However, on wet or rainy asphalt, μ can decrease to 0.7, and in snow or ice, the value of μ can be as low as 0.2 [16]. Another insight from Figure 1.1 is the coupled relationship between vehicle lateral and longitudinal forces. If the vehicle is braking (or accelerating) heavily, the value of F_x^2 will be large and there will be less friction force available for turning.

1.2.1 Exceeding the Friction Limits: Understeer and Oversteer

In normal driving situations, the forces required for turning, braking, and accelerating will be much smaller than the available friction force. However, in rainy or

icy conditions, accidents frequently occur when the driver enters a turn too fast or when the driver attempts to turn too quickly while already applying the brakes. In these situations, the tire forces at either the front or rear axle become saturated, resulting in one of two distinct scenarios.

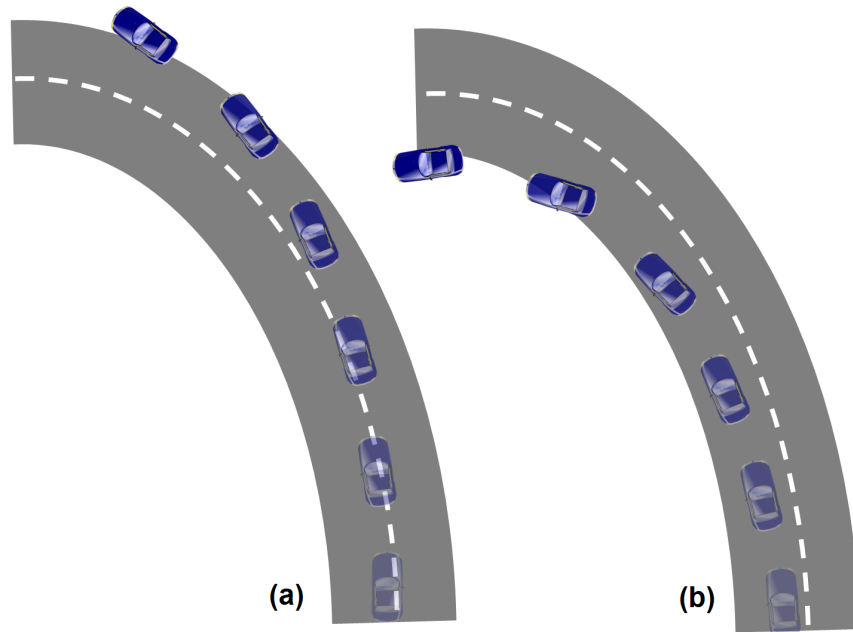


Figure 1.2: (a) Vehicle understeering at the limits of handling. (b) Vehicle oversteering at the limits of handling

When the front tire forces become saturated, the vehicle will understeer, as illustrated in Figure 1.2. The steering actuator of a vehicle only has direct control of the front tire forces. As a result, additional turning of the steering wheel will not generate additional lateral force or acceleration when the front axle is saturated. The vehicle therefore becomes uncontrollable and has no ability to reduce the radius of its turn. For the converse scenario where the rear tire forces become saturated, the vehicle enters an oversteer condition, as illustrated in Figure 1.2.

In this situation, the vehicle loses stability and begins to spin. An oversteer situation differs from an understeer because the front tire forces are not saturated, and the steering actuator can therefore be used to fully control the vehicle. As a result, it is possible to apply a countersteer maneuver to reverse the vehicle spin and gain control of the vehicle without deviating from the desired path.

1.3 State of the art

In recent years a lot of researches have been focused on autonomous racing and, for this reason, an overview of the existing projects has been done at the beginning of this work. In particular, the state of the art regarding the development of the vehicle control for autonomous racing has been analysed.

The design of MPC-based controllers for racing applications have been described on a 1:43 RC cars platform [17]. The work focuses on providing two approaches for the design of real-time optimal racing controllers: a 1-layer MPC and a 2-layers MPC formulation. The setup consists in a controller-equipped car placed in a defined racing track, both previous formulations being implemented and compared in two scenarios: with and without obstacles on the track. The 2-layers approach combines a path planner relying on a car model derived with simplifying assumptions providing both optimal path and associated car velocity, and a path tracker steering the car towards the previously generated path. Both tasks use a MPC formulation: the path planner optimizes the progress along the centerline and the path tracker minimizes the deviation of the car from the optimal path. The 1-layer approach defines a contouring error whose minimization results in maximizing the progress along the centerline. The conclusion of this study suggests that both approaches have pros and cons. The 2-layers approach being sensitive to unfeasible path generation because of the path planner relying on a simplified car model, and the 1-layer approach tendency to track the centerline are amongst the known issues. A different design is suggested in [18], taking advantage of a reformulation of the whole racing problem to set the racing time as the objective function. The results suggest that this method allows for both an optimal racing behaviour and the tuning of holistic driving strategy variables such as the aggressivity of the driver. Other nonlinear optimal formulations are described in [19]. The goal is to design a side wind rejection feature using a MPC controller relying on an advanced car model integrating tyre modelling to control the car even in a low adherence scenario (drift). Conclusions indicate that the real-time implementation of such complex formulations is however hard to achieve.

A solution to that issue is suggested in [20]. A simple dynamic model using a second order integrator dynamics is designed and scaled to specific actual vehicles using a sequence of experiments to derive the set of model parameters by curve fitting. The

authors indicate that this model can be used for near-limits path planning applications and the conclusions of the study suggest that the accuracy provided by this approach would be sufficient. Another approach is taken in [21], where kinematic and dynamic bicycle models are compared taking into account the discretization phenomena. Results suggest that a controller using the discrete kinematic (simpler) model would perform similarly to its counterpart using a dynamic model, at the condition of using a lower sampling rate.

The topic of vehicle stabilization around a path is addressed in [22], model linearization is used to achieve the same goal as the previous study in a lane-change scenario. Physical limits of the car are taken into account to provide a stable control. Near-limits dynamic control offer serious challenges because of the complex dynamics of a car tyre in case of adherence loss. Classic control methods are used to tackle this issue in [23]. Combining lateral (path tracking) and longitudinal (speed profile generation) controllers, both taking advantage of feedback and feed-forward schemes, real-time asymptotically stable controllers are designed. Conclusions suggest that it is possible to drive a car at its friction limits using this controller.

Offline methods are suggested in [24] for the path tracking task. A Linear Quadratic Regulation (LQR) controller is derived and implemented to minimize the path tracking error in a lane-change situation. A comparison is made between this methods and other classic designs. The results suggest that a fine tuning of such controllers can provide satisfactory results for different applications such as slow driving or highway driving.

Instead, in [20], a computationally light way of sampling feasible acceleration regions for the car. Starting from a known state, the future car positions can be computed through numerical integration. The first step is to compute a set of feasible longitudinal, lateral and angular accelerations for various initial states of the vehicles in an off-line fashion. This region is then approximated to a linear convex one. The Figure shows the result of such computation. One of the perks of this approach is not to be limited to stationary trajectories. Finally, an original bicycle kinematic model is derived using a road-aligned approach [25]. The obtained linear system is then used to derive an obstacle avoidance car controller.

In this thesis, a coupled lateral and longitudinal controller for autonomous racing based on an adaptive MPC is proposed. The proposed control strategy maximizes

the longitudinal speed while remaining in constrained speed range and without exceeding the adherence condition. At the same time, it eliminates the path error between the actual location and the desired path in terms of lateral deviation and desired yaw angle, assuring the handling stability during the motion. The command signals generated by MPC and provided to the vehicle are the front wheel steering angle and actuation of throttle/brake pedals.

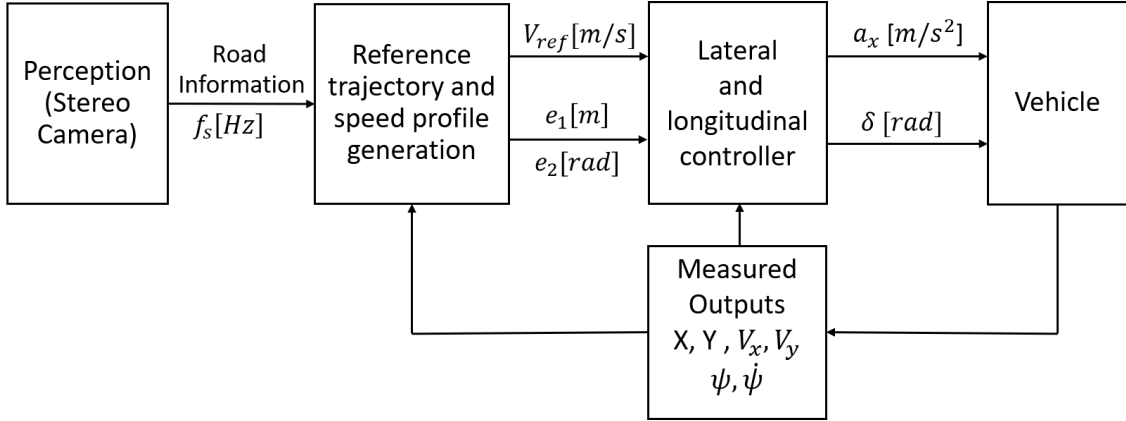


Figure 1.3: Global architecture of control strategy for autonomous driving presented in this thesis

The overall autonomous racing system has been implemented with MATLAB and Simulink¹. The technique exploits a simulated stereo camera that utilizes the synthetic data coming from the simulated driving scenario for lane detection, as shown in Figure 1.3. In the real implementation, this information is obtained from a lane detection algorithm based on the real-time streaming of a stereo-camera data. Since, in our case the simulations are conducted in MATLAB/Simulink, the lane boundaries information is extracted from simulated racing scenarios. Dynamics of the vehicle is modeled using a 3 degree of freedom rigid vehicle model.

¹<https://it.mathworks.com/>

1.4 Thesis outline

The thesis is organized as follows:

- *Chapter 2*: It presents the vehicle modeling used for the validation and control synthesis. In particular, a 3 degree of freedom rigid vehicle model, tire model, driveline dynamics and a linearized vehicle model for MPC control design are discussed in detail.
- *Chapter 3*: First, Perception, Reference trajectory and speed profile generation presented. Later MPC control design explained in detail and discussed about other two controllers.
- *Chapter 4*: Three different controllers are presented to evaluate the performance by means of simulations. The results are presented and discussed.
- *Chapter 5*: In the final chapter conclusions and future works are reported.

Chapter 2

Modelling

There are different types vehicle models, each meant for a specific purpose. The system elements or components of the vehicle model governs its behaviour. For example, a quarter model (one or two degrees of freedom (DOF) vertical model), for studies towards vertical dynamics, like active suspension as in [26] or 14DOF model that is suitable for Roll dynamics study [27]. There are other detailed vehicle models with 38 DOF [28] or multibody models available within commercial software packages with more than 100 DOF. The degree of detail required on the model is determined by the application. Before looking into different types of vehicle models it is important to know the various system elements that compose a complete vehicle model. They are: 1. Vehicle body 2. Wheel and Tires 3. Powertrain 4. Suspension 5. Steering 6. Brakes 7. Vehicle control

As discussed previously, vehicle models serve a certain purpose based on which they are classified as follows:

- Vertical dynamics model
- Longitudinal and lateral dynamics model
- Full dynamics model

For this thesis, we are considering the Longitudinal and lateral dynamics model. in which, the motion of the vehicle is investigated in the yaw plane mainly describing the longitudinal and lateral vehicle motion. In the description of the vehicle motion, different longitudinal and lateral dynamic couplings must be considered:

- Dynamic and kinematic couplings are due to the motion in the yaw plane caused by wheels steering.
- The interaction between tyre and road is at the origin of another important coupling. In fact, the maximal available tyre-road friction is distributed between lateral and longitudinal tyre forces. This distribution is governed by the well known friction ellipse [29].
- The longitudinal and lateral accelerations cause a load transfer between the front and rear axles as well as the right and left wheels. These load transfers affect the vertical dynamics as well as the lateral and longitudinal ones due to the modification in the normal tyre forces.

Model-based control is highly affected by the quality of the models provided. On the one hand, accurate models are typically computationally expensive and provide accurate predictions. On the other hand, simple models are less computationally demanding, but provide less accurate predictions. Since the MPC will be evaluated through simulations, a validation model is needed. The validation model needs to well describe the behaviour of a real vehicle. So, for this thesis, dynamics of the vehicle is modeled using the 3 degree of freedom rigid vehicle model (dual Track), which is imported from Vehicle dynamics Blockset in Simulink®. The derivation of the kinematic and the dynamic vehicle model is described in Section 2.1.1 and 2.1.2. For this thesis we used a linearized dynamic model of the vehicle, derived in Section 2.3, as the prediction model.

2.1 Vehicle model for validation and simulation

In this section, both kinematic and dynamic models of the vehicle are presented with their assumptions and constraints.

2.1.1 Kinematic model

The simplest approach to the vehicle motion is to consider a vehicle moving on a horizontal plane with 3 Degree of Freedom (DOF), the two displacements on the plane (longitudinal and lateral) and the rotation around an axis normal to that plane (yaw rotation). By controlling these 3 DOF over time, the vehicle's trajectory

will be known, so the path described by the vehicle can be studied. If additional simplifications are made, considering that the vehicle travels at constant speed and the trajectory radius when turning is much larger than the vehicle's track width, this model can be represented by a two-wheeled vehicle model, usually known as Single-track. Bicycle model The model's equations are derived from [32]. As shown in Figure 2.1, the following kinematic model of the vehicle has been considered [30].

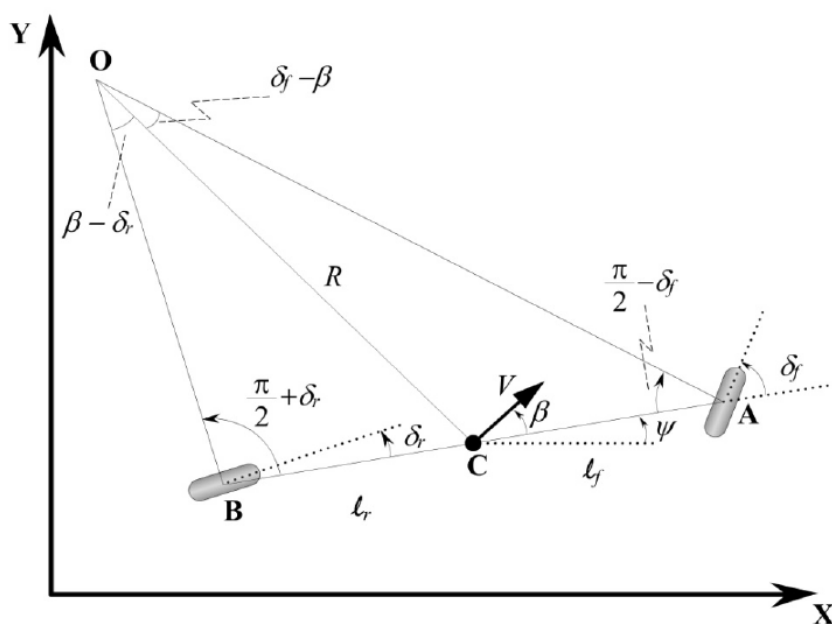


Figure 2.1: Vehicle kinematic model

The image presents a bicycle model in which the two front wheels and the two rear wheels are represented by one single central tires at points A and B, respectively. The steering angle for the front wheel is indicated with δ_f , while δ_r refers to the steering angles for the rear wheel. In this work, the vehicle model is assumed as a front-wheel-only steering, therefore the rear steering angle δ_r is set to zero. The point C in the figure represents the center of gravity (c.g.) of the vehicle. The distances from this point to the points A and B are indicated with l_f and l_r respectively. The sum of these two terms corresponds to the wheelbase L of the

vehicle:

$$L = l_f + l_r \quad (2.1)$$

Since the vehicle is assumed to have planar motion, three coordinates are necessary to describe the vehicle motion: X , Y and Ψ . (X , Y) represent the inertial coordinates of the location of the center of gravity of the vehicle, while Ψ indicates the orientation of the vehicle and it is called yaw angle. The vector V in the model refers to the velocity at the c.g. of the vehicle. This vector makes an angle β , called slip angle, with the longitudinal axis of the vehicle.

The point O refers to the instantaneous center of rotation of the vehicle and it is defined by the intersection of lines AO and BO . These two lines are drawn perpendicular to the orientation of the two wheels. The length of the line OC corresponds to the radius of the vehicle trajectory R , and it is perpendicular to the velocity vector V .

Applying the sine rule to triangles OCA and OCB , remembering that δ_r is equal to zero, it is possible to define the following equations:

$$\frac{\sin(\delta_f - \beta)}{l_f} = \frac{\sin(\frac{\pi}{2} - \delta_f)}{R} \quad (2.2)$$

$$\frac{\sin(\beta)}{l_r} = \frac{1}{R} \quad (2.3)$$

After some manipulation and multiplying by $\frac{l_f}{\cos(\delta_f)}$, equation 2.2 becomes:

$$\tan(\delta_f) \cos(\beta) - \sin(\beta) = \frac{l_f}{R} \quad (2.4)$$

Likewise, multiplying by l_r , equation 2.3 can be re-written as:

$$\sin(\beta) = \frac{l_r}{R} \quad (2.5)$$

Adding equations 2.4 and 2.5, the following relation has been obtained:

$$\tan(\delta_f) \cos(\beta) = \frac{l_f + l_r}{R} \quad (2.6)$$

This formula allows to write the radius R of the vehicle trajectory as a function of the front steering angle δ_f , the slip angle β , and l_f .

If the value of radius R changes slowly due to low velocity, the yaw rate $\dot{\Psi}$ of the vehicle can be assumed equal to the angular velocity ω that is defined as:

$$\omega = \frac{V}{R} \quad (2.7)$$

Therefore, the yaw rate $\dot{\Psi}$ can be described as follows:

$$\dot{\Psi} = \frac{V}{R} \quad (2.8)$$

Using formula 2.6, the equation 2.8 can be re-written as:

$$\dot{\Psi} = \frac{V \cos(\beta)}{l_f + l_r} \tan(\delta_f) \quad (2.9)$$

After all these assumptions, the overall equations of the kinematic model can be defined as:

$$\dot{X} = V \cos(\Psi + \beta) \quad (2.10)$$

$$\dot{Y} = V \sin(\Psi + \beta) \quad (2.11)$$

$$\dot{\Psi} = \frac{V \cos(\beta)}{l_f + l_r} \tan(\delta_f) \quad (2.12)$$

2.1.2 Dynamic model

A kinematic model offers satisfactory results when the vehicle speed and steering angle are low enough, but it becomes inadapted when the vehicle is brought to its limit of adherence and tires start to lose grip on the road (this is referred as drifting). To simulate a realistic vehicle behaviour, it is necessary to integrate these complex dynamics in our simulation model. Moreover, a simplified version of these dynamics can be integrated to the prediction model to allow the controller to predict when the tires are about to lose grip..

In this thesis, dynamics of the vehicle is modeled using the 3 degree of freedom rigid vehicle model (dual Track), which is imported from Vehicle dynamics Blockset in Simulink [31]. This model accounts for the two displacements on the plane (longitudinal, depicted by subscript x and lateral depicted by subscript y) and the rotation around an axis normal to the plane (yaw motion). It implements a rigid two axle vehicle body model. So, As our test vehicle is only steerable from the front wheels, the test vehicle is modeled to be only steerable from the front wheel.

Let x and y respectively be the longitudinal and lateral directions in the vehicle frame, X and Y the longitudinal and lateral directions in the absolute frame, ψ the yaw angle in the x, y frame and the heading angle in the X, Y frame.

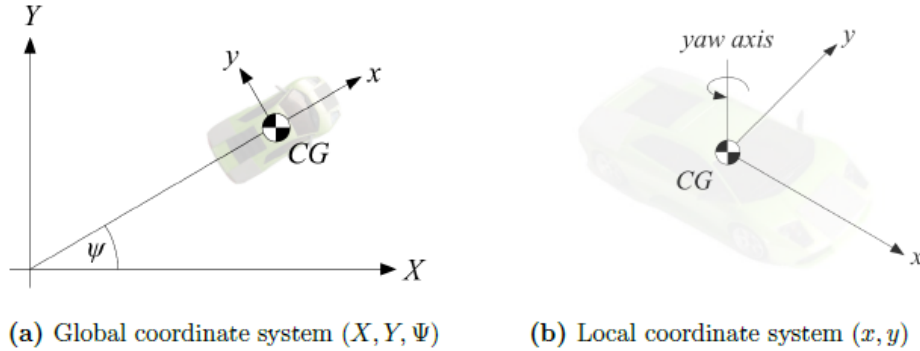


Figure 2.2: Model Coordinate Systems

The nomenclature refers to the model depicted in Figure 2.3. denote by F_l, F_c the longitudinal (or “tractive”) and lateral (or “cornering”) tire forces, respectively, F_x, F_y the longitudinal and lateral forces acting on the vehicle center of gravity, F_z the normal tire load, X, Y the absolute car position in inertial coordinates, $l_f,$

l_r (distance of front and rear wheels from center of gravity), g the gravitational constant, m the car mass, I_{zz} the car inertia, α the slip angle, δ the wheel steering angle and Ψ the heading angle. The lower scripts f and r particularize a variable at the front wheels and the rear wheels, respectively, e.g. F_{lf} is the front wheel longitudinal force. we will use two subscript symbols to denote variables related to the four wheels. In particular the first subscript denotes the front and rear axles, the second denotes the left and right sides of the vehicle. As example, the variable $(.)_{f,l}$ is referred to the front left wheel.

Newton Euler equations (2.13), (2.14) denote the longitudinal and lateral momentum with respect to CG in the vehicle reference frame while yaw dynamics are considered by (2.15). the following dynamic model of the vehicle has been considered [33][34].

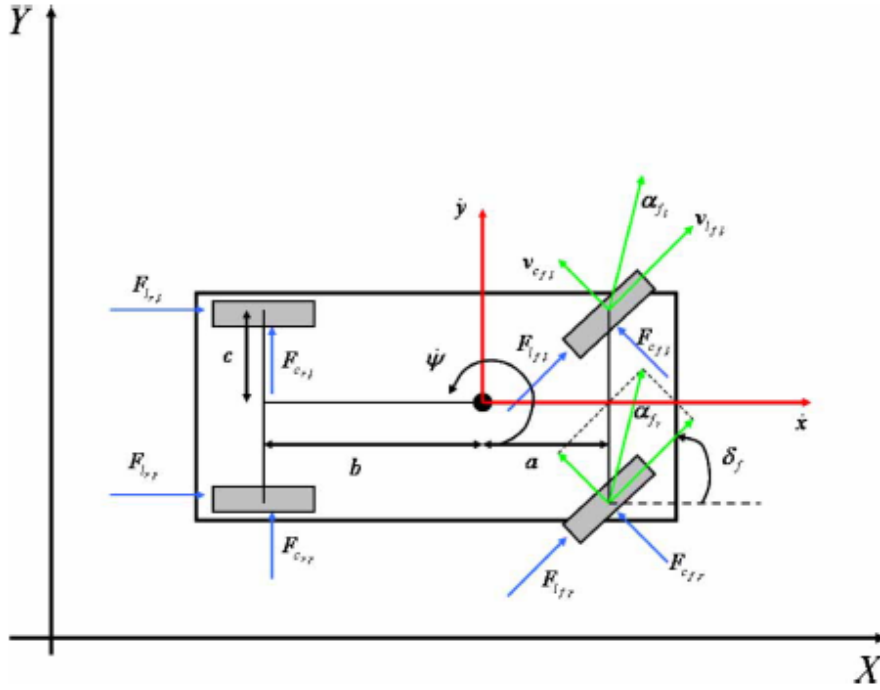


Figure 2.3: 3 DoF rigid vehicle model

$$m\dot{V}_x = mV_y\dot{\Psi} + F_{xf,l} + F_{xf,r} + F_{xr,l} + F_{xr,r} + F_{x,ert} \quad (2.13)$$

$$m\dot{V}_y = -mV_x\dot{\Psi} + F_{yf,l} + F_{yf,r} + F_{yr,l} + F_{yr,r} + F_{y,ext} \quad (2.14)$$

$$I_{zz}\ddot{\Psi} = a(F_{yf,l} + F_{yf,r}) - b(F_{yr,l} + F_{yr,r}) + c(-F_{xf,l} + F_{xf,r} - F_{xr,l} + F_{xr,r}) + M_{z,ext} \quad (2.15)$$

The vehicle's equations of motion in an absolute inertial frame are

$$\dot{X} = \dot{x} \cos \Psi - \dot{y} \sin \Psi \quad (2.16)$$

$$\dot{Y} = \dot{x} \sin \Psi + \dot{y} \cos \Psi \quad (2.17)$$

The longitudinal and lateral forces generated by the four tyres lead to the following components along the lateral and longitudinal vehicle axes:.

$$F_x = F_l \cos \delta - F_c \sin \delta \quad (2.18)$$

$$F_y = F_l \sin \delta + F_c \cos \delta \quad (2.19)$$

For the sake of simplicity, the steering angles of the left and right front wheels are supposed to be equal. Assuming front wheels drive, the dynamic of the wheels involving front and rear axle can be described as below:

$$J_{w,f}\dot{\omega}_f = T_w - T_b - r_w F_{l,f} \quad (2.20)$$

$$J_{w,r}\dot{\omega}_r = -T_b - r_w F_{l,r} \quad (2.21)$$

where J_w is moment of inertia of the wheels, $\dot{\omega}$ is the angular acceleration of the wheel, T_w is the wheel torque and T_b is brake torque. The subscript r and f denote the rear and front wheel respectively.

2.2 Tire models

Several years an impressive amount of research has been done regarding tire behavior and modeling, ending up with several different types of tire models with different characteristics[35]. An extended classification of tire models is based on the differ-

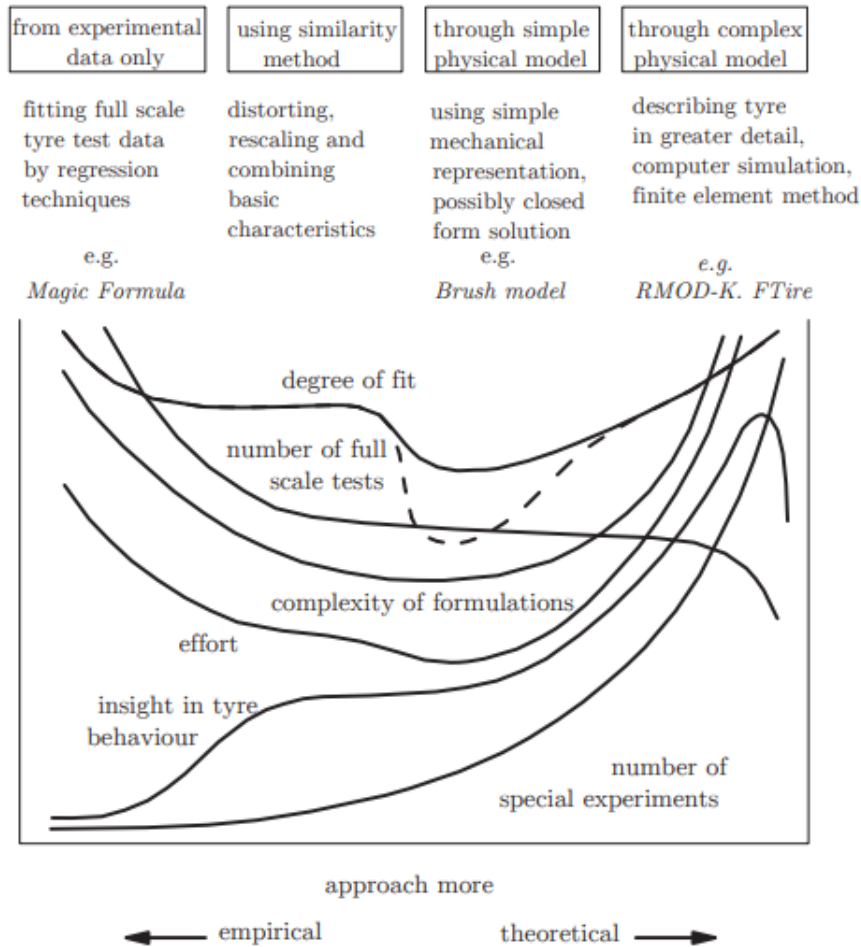


Figure 2.4: Classification of tire models

ent approaches used to develop the models, which can go from a completely empiric view, mainly fitting full scale tire test data by regression techniques, to fully theoretical tire models, usually based on its structural behavior study through finite element simulations. Between these two extremes, a bunch of models combining theoretical solutions with empirical measurements in different levels have been developed. Typically, empirical models are over parameterized and as a consequence

it is hard to use them in domains where there are no measurements available, e.g. when using in combined slip situation a tire model fitted with pure lateral and longitudinal measurement data. On the other hand, these models are often very compact, usually some analytical equations, and computationally fast, which can be a great advantage for real-time simulation. Theoretical models describe the tire behavior in great detail, usually including most of the steady-state and transient phenomenon affecting the tire response, but this level of detail means that simulating these models is a computational heavy task. Full theoretical models are often used to develop new tires but they have no practical application for complete vehicle simulation.

Finally, one can identify the middle ground in the so-called Semi-empirical tire models, which include tire models specially developed to represent the tire as a component of a vehicle in a simulation environment. These models are based on measured data but also may contain structures and strategies used in theoretical models, presenting a good balance between accuracy and computation speed [35].

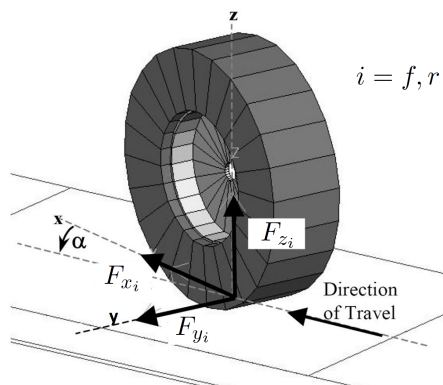


Figure 2.5: Illustration of the tire model

The tire forces have highly nonlinear behavior when slip ratio or slip angle is large. Thus it is of extreme importance to have a realistic nonlinear tire force model for the vehicle dynamics when operating the vehicle in the tire nonlinear region e.g. during racing. In such situations, large slip ratio and slip angle can happen simultaneously and the longitudinal and lateral dynamics of the vehicle is highly coupled and nonlinear due to the nature of the tire forces. Similar situation can occur even with small inputs when the surface friction coefficient μ is small.

Tires are one of the most important components of vehicles, since they are the

only component keeping the vehicle in contact with the ground. The primary force generated between the tire and the road interface push the vehicle forward during acceleration(traction force) and reduces the speed of the vehicle during braking (braking effort). This force is known as the longitudinal force. Except for aerodynamic, gravity and rolling resistance forces, all of the other forces which affect vehicle handling are produced by the tires as depicted in Figure 2.5

Before introducing sophisticated tire model, firstly some terms related to tire model have been defined in following. The front and rear tire speeds along x-axis and y-axis are calculated as below

$$v_{x,i} = v_i \cos\alpha_i \quad (2.22)$$

$$v_{y,i} = v_i \sin\alpha_i \quad (2.23)$$

where v_f and v_r are the front and rear tire speed, α_f and α_r are the front and rear tire slip angle. The correlation between tire speeds and host vehicle speed is given below

$$v_{x,f} = v_{h,x} \quad (2.24)$$

$$v_{x,r} = v_{h,x} \quad (2.25)$$

$$v_{y,f} = v_{h,y} + l_f \dot{\Psi} \quad (2.26)$$

$$v_{y,r} = v_{h,y} - l_r \dot{\Psi} \quad (2.27)$$

The slip angle represents the angle between the wheel velocity and the direction of the wheel itself [6]. Then tire side-slip angles are computed as

$$\alpha_f = \delta_f - \frac{v_{y,f}}{v_{x,f}} \quad (2.28)$$

$$\alpha_r = \delta_r - \frac{v_{y,r}}{v_{x,r}} \quad (2.29)$$

The tire forces depend on the tire side-slip values and on the friction characteristics between the road and the tires. The longitudinal wheel-slip ratio, which refers to the difference in angular speed between a purely rolling wheel and a wheel that also slides, is defined for each tire as

$$\sigma_i = \frac{r w_i - v_{x,i}}{v_{x,i}} \quad r w_i < v_{x,i} \quad \textit{Braking} \quad (2.30)$$

$$\sigma_i = \frac{r w_i - v_{x,i}}{r w_i} \quad r w_i > v_{x,i} \quad \textit{driving} \quad (2.31)$$

where w_f and w_r are the angular velocities of front and rear tires, r is the radius of wheels and $i = f, r$.

The maximum function in the denominator of the above equation allows its use for both acceleration and braking models. A slip ratio equal to zero means that the forward velocity and tire rolling speed are equal, which implies an absence of either engine or brake torque. A positive slip ratio implies that the tire has a positive finite rolling velocity, and the vehicle possesses a greater finite forward velocity. A negative slip ratio implies that the vehicle has a finite forward velocity and the tire has a greater equivalent positive rolling velocity. At each extreme, i.e. +1 and - 1, the wheel is either "locked" at zero speed, or "spinning" with the vehicle at zero speed. When both tire and vehicle velocity are equal to zero, the slip is mathematically undefined, and is taken to be zero for simulation purposes. Experimental studies have produced several clearly defined friction/slip characteristics between the tire and road surface for a variety of different driving surfaces and conditions[36]

2.2.1 Pacejka tire model

It is a complex nonlinear semi-empirical model being able to describe the nonlinear and coupled behavior of tire forces under wide operation range. Pacejka model describes the tire forces as functions of the tire normal force, slip ratio, slip angle and surface friction coefficient [37].

It is critical to have a realistic tire model to take the slip phenomenon into account, without that it would not be possible to drive the car at its limits of handling and race efficiently. It is valuable to calculate the lateral and the longitudinal forces acting as a function respectively of the lateral slip angle α and slip ratio,

2.2.2 Logitudinal Tire Forces

In this model the longitudinal forces are assumed to depend on the normal force, surface friction, and longitudinal slip ratio as shown below

$$F_{x,i} = F_x(\sigma_i, \mu, F_{z,i}) \quad (2.32)$$

Pacejka tire model is utilized to calculate longitudinal force based on the percent longitudinal slip. The Pacejka model which was applied to calculates the friction coefficient as a function of logitudinal slip ratio:

$$\mu(\sigma) = D \sin(C \tan^{-1}(B\sigma - E(B\sigma - \tan^{-1}(B\sigma)))) \quad (2.33)$$

The value of B , C , D and E for different road types are shown in Table 2. The model defines in excess of 40 constants that are determined from the given set of experimental data, and the overall model coefficients B , C , D and E are then calculated from a combination of these constants. Having the friction coefficient

Table 2. Coeffients of the Pacejka model for different road condition

Surface	B	C	D	E
Dry Tarmac	10	1.9	1	0.97
Wet Tarmac	12	2.3	0.82	1
Snow	5	2	0.3	1
Ice	4	2	0.1	1

Figure 2.6: Coeffients of the Pacejka model for different road condition

$\mu(\sigma)$ and the normal force F_z exerting on the wheel, the longitudinal traction force

F_x is then calculated as follows:

$$F_x = \mu(\sigma) F_z \quad (2.34)$$

2.2.3 Lateral Tire Forces

Highly nonlinear behavior of tire forces cause the large variation in vehicle handling properties throughout the longitudinal and lateral maneuvering range. In some literature, Lateral tire forces which are crucial for maneuvering capability of the vehicle are assumed to depend on the normal force, surface friction, and slip angle.

$$F_{y,i} = F_y(\alpha_i, \mu, F_{z,i}) \quad (2.35)$$

This is due to the experimental data obtained from the vehicle tires as shown in 2.7. It can be seen that at low slip angles (which is found to be 5 deg or less by [39] and [40]), the lateral forces F_y vary proportionally to the slip angle α . The transitional region is the region where maximum tire forces exist (usually 4 deg 6 deg). Typical Anti-Lock Braking Systems (ABS) try to keep slip angle with-in this maximum force region to obtain maximum possible braking force. In the frictional region, the tire starts skidding and it can not provide as much lateral force. Cornering Stiffness C_f is defined as the ratio between F_y and α . Subscript f and r denote front and rear tire respectively. SAE defines cornering stiffness as modulus of the slope which means it can never be negative [41]. Cornering stiffness depends upon the manufacturing features of the tire e.g., radius, width, tread, inflation pressure etc. In this research, this linear model of tire lateral dynamics will be used since it is very simple (hence suitable for online application) as compared to complex tire models and at the same time sufficiently accurate. Slip angle commutes in linear region as shown in Figure 2.7, lateral tire forces are linear functions of slip angles, cornering stiffnesses of the tire [42]:

$$F_{y,i} = 2C_{y,i}\alpha_i \quad (2.36)$$

where $C_{y,i}$ are the cornering stiffness. The factor 2 in Equation accounts for the fact that there are 2 tires per axle in the bicycle model adopted. The cornering stiffness are defined for the front and rear tires based on the static distribution of

weight between the front and rear axles as [43].

$$C_{y,i} = C_s \frac{F_{z,i,static}}{2} \quad (2.37)$$

where C_s is the cornering stiffness coefficient

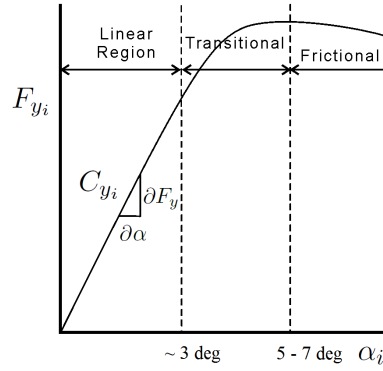


Figure 2.7: Lateral tire force regions

As shown in Figure 2.8, the front wheel slip angle α_f can be defined as the difference between the steering angle δ of the front wheel and the orientation angle of the tire velocity vector θ_{V_f} with respect to the longitudinal axis of the vehicle.

$$\alpha_f = \delta - \theta_{V_f} \quad (2.38)$$

In a similar way, the rear wheel slip angle is defined as:

$$\alpha_r = -\theta_{V_r} \quad (2.39)$$

Therefore, the lateral tire forces for the front and rear wheels of the vehicle is obtained as:

$$F_{y_f} = 2C_{\alpha_f}(\delta - \theta_{V_f}) \quad (2.40)$$

$$F_{y_r} = 2C_{\alpha_r}(-\theta_{V_r}) \quad (2.41)$$

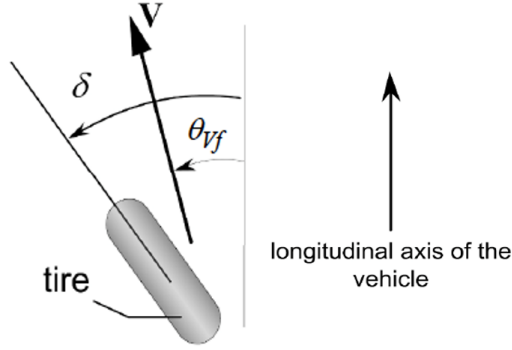


Figure 2.8: Tire slip angle

where $C_{\alpha f}$ and $C_{\alpha r}$ are proportional constants. These constants are called cornering stiffness of front and rear wheel respectively. The factor 2 in the equations refers to the fact that there are two wheels for each axle.

In order to calculate the velocity angle of the front wheel θ_{Vf} and the rear wheel θ_{Vr} , the following formulas have been used:

$$\tan(\theta_{Vf}) = \frac{V_y + l_f \dot{\Psi}}{V_x} \quad (2.42)$$

$$\tan(\theta_{Vr}) = \frac{V_y - l_r \dot{\Psi}}{V_x} \quad (2.43)$$

Assuming small angle approximations, the equations 2.42 and 2.43 can be re-written as:

$$\theta_{Vf} = \frac{V_y + l_f \dot{\Psi}}{V_x} \quad (2.44)$$

$$\theta_{Vr} = \frac{V_y - l_r \dot{\Psi}}{V_x} \quad (2.45)$$

Substituting above set of Equations in 2.46 and 2.47 gives us the final relationship of tire longitudinal forces:

$$F_{yf} = 2C_{\alpha f} \left(\delta - \frac{V_y + l_f \dot{\Psi}}{V_x} \right) \quad (2.46)$$

$$F_{yr} = 2C_{\alpha r} \left(-\frac{V_y - l_r \dot{\Psi}}{V_x} \right) \quad (2.47)$$

The longitudinal and lateral tire force $F_{x,i}$, $F_{y,i}$ are limited physically by the adhesion limit between tire and road [32]. Because the contact patch can induce a maximum force, if a certain force is applied in longitudinal direction the maximum possible force in lateral direction is reduced. Therefore, the tire forces always lie inside the following ellipse. Therefore, during combined slip conditions the maximum transferred force is given by

$$\sqrt{F_x^2 + F_y^2} < \mu F_z \quad (2.48)$$

2.3 Vehicle model for MPC

In this thesis work, the goal is to implement a combined lateral and longitudinal control system based on MPC for autonomous racing. For this purpose, a 2 degree of freedom vehicle model is used to define the lateral dynamics of the vehicle for controller internal plant model in terms of error with respect to the reference trajectory. The two errors are lateral displacement error e_1 , which is defined as the lateral distance between center of gravity of vehicle and the center line of the reference trajectory. Yaw angle error e_2 is defined as the difference between the yaw angle of the vehicle and desired yaw angle as dictated by the reference trajectory, as represented in Figure 2.9. The rate of change of lateral displacement error and yaw angle error are given by the equations.

$$\dot{e}_1 = V_x e_2 + V_y \quad (2.49)$$

$$e_2 = \Psi - \Psi_{des} \quad (2.50)$$

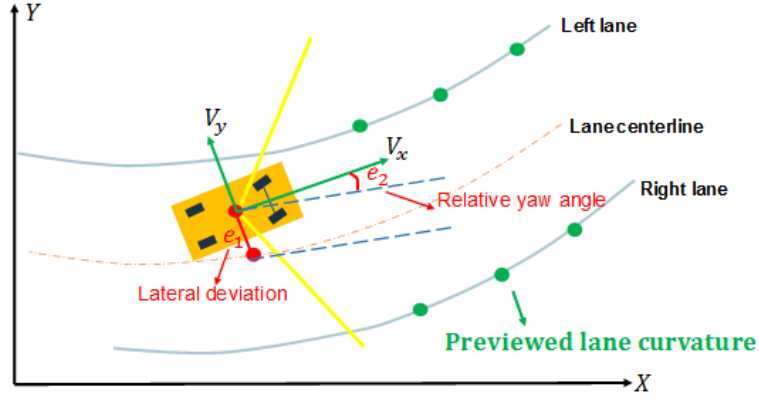


Figure 2.9: Bicycle model in terms of lateral deviation and relative yaw angle with respect to the center line of the lane

The desired yaw angle rate is given by:

$$\dot{\Psi}_{des} = V_x \kappa \quad (2.51)$$

Where, κ denotes the the road curvature.

The state-space model for lateral dynamics can be obtained by linearizing the bicycle model described in section 2.1.2. $\dot{x} = Ax + Bu$ is represented as:

$$\begin{bmatrix} \dot{y} \\ \dot{\Psi} \\ \ddot{\Psi} \end{bmatrix} = \begin{bmatrix} 0 & 1 & 0 & 0 \\ 0 & -\frac{2C_{\alpha f} + 2C_{\alpha r}}{mV_x} & 0 & -V_x - \frac{2C_{\alpha f}L_f - 2C_{\alpha r}L_r}{mV_x} \\ 0 & 0 & 0 & 1 \\ 0 & -\frac{2L_f C_{\alpha f} - 2L_r C_{\alpha r}}{I_z V_x} & 0 & -\frac{2L_f^2 C_{\alpha f} + 2L_r^2 C_{\alpha r}}{I_z V_x} \end{bmatrix} \begin{bmatrix} y \\ \dot{\Psi} \\ \ddot{\Psi} \end{bmatrix} + \begin{bmatrix} 0 \\ \frac{2C_{\alpha f}}{m} \\ 0 \\ \frac{2L_f C_{\alpha f}}{I_z} \end{bmatrix} \delta \quad (2.52)$$

For the longitudinal dynamics, the plant model used for control design is the transfer function between desired acceleration and actual vehicle speed and is given by[32]:

$$P(s) = \frac{1}{s(\tau s + 1)} \quad (2.53)$$

Where, τ is the time constant. Due to the finite bandwidth associated with the lower controller, the vehicle is expected to track its desired acceleration imperfectly. Thus there is a first order lag in the lower level controller performance and hence the use for the upper controller which incorporates a lag in tracking desired acceleration.

The lag in the performance of the lower controller comes from several sources, accumulating brake or engine actuation lags and sensor signal processing lags.

- The pure time delay in the engine response (60 milliseconds at 2000rpm),
- The bandwidth of the lower level multiple-sliding-surface controller that tracks acceleration
- The bandwidth of low pass filters used for other sensors such as engine manifold pressure sensor, wheel speed sensor, etc
- The bandwidth of the throttle actuator
- The lag due to discrete sampling at 50 Hz (20 ms sampling)
- The 200 ms lag due to the radar filter
- When braking, the brake actuator lag instead of engine time delay.

overall time constant of the lower level controller could be as much as 500 milliseconds.

A traditional MPC controller includes a nominal operating point at which the plant model applies, such as the condition at which you linearize a nonlinear model to obtain the LTI approximation. If the plant is strongly nonlinear or its characteristics vary dramatically with time, LTI prediction accuracy might degrade so much that MPC performance becomes unacceptable. Adaptive MPC can address this degradation by adapting the prediction model for changing operating conditions. As described in the Model Predictive Control Toolbox™, adaptive MPC uses a fixed model structure, but allows the model parameters to evolve with time. Ideally, whenever the controller requires a prediction (at the beginning of each control interval) it uses a model appropriate for the current conditions. So, in an adaptive MPC, the plant model is updated at each time step as the operating point keeps changing. i.e. Vehicle longitudinal speed. The plant model used as the basis for adaptive MPC is an LTI discrete-time, state-space model with a sampling time $T_s = 100$ ms. The combined state space model for lateral and longitudinal dynamics

which is used as the internal plant model for MPC is represented below:

$$\begin{aligned} x(k+1) &= Ax(k) + B_u u(k) + B_d v(k) \\ z(k) &= Cx(k) \end{aligned} \quad (2.54)$$

Where:

- k is time index (current control interval).
- x are plant model states.
- u are manipulated inputs. These are the one or more inputs that are adjusted by the MPC controller.
- v are measured disturbance inputs.
- A is the state matrix.
- B_u and B_d are the input matrices corresponding to inputs u and v respectively
- C is the output matrix.

$$\begin{bmatrix} \ddot{V}_x \\ \dot{V}_x \\ \dot{V}_y \\ \ddot{\psi} \\ \dot{e}_1 \\ \dot{e}_2 \end{bmatrix} = \begin{bmatrix} \frac{-1}{\tau} & 0 & 0 & 0 & 0 & 0 \\ 1 & 0 & 0 & 0 & 0 & 0 \\ 0 & 0 & -\frac{2C_{\alpha f} + 2C_{\alpha r}}{mV_x} & -V_x - \frac{2C_{\alpha f}L_f - 2C_{\alpha r}L_r}{mV_x^2} & 0 & 0 \\ 0 & 0 & -\frac{2L_f C_{\alpha f} - 2L_r C_{\alpha r}}{I_z V_x} & -\frac{2L_f^2 C_{\alpha f} + 2L_r^2 C_{\alpha r}}{I_z V_x} & 0 & 0 \\ 0 & 0 & 1 & 0 & 0 & V_x \\ 0 & 0 & 0 & 1 & 0 & 0 \end{bmatrix} \begin{bmatrix} \dot{V}_x \\ V_x \\ V_y \\ \dot{\psi} \\ e_1 \\ e_2 \end{bmatrix} + \begin{bmatrix} \frac{1}{\tau} & 0 \\ 0 & 0 \\ 0 & \frac{2C_{\alpha f}}{m} \\ 0 & \frac{2L_f C_{\alpha f}}{I_z} \\ 0 & 0 \\ 0 & 0 \end{bmatrix} \begin{bmatrix} a_x \\ \delta \end{bmatrix} + \begin{bmatrix} 0 \\ 0 \\ 0 \\ 0 \\ 0 \\ -V_x \end{bmatrix} [\rho] \quad (2.55)$$

The inputs for the plant are separated to indicate that u correspond the front wheel steering angle and acceleration/deceleration command of the vehicle (controlled output of MPC), while v indicates the longitudinal velocity multiplied by the curvature κ (it is the disturbance). The inputs to the MPC y corresponds to the lateral deviation e_1 , relative yaw angle e_2 and velocity of the vehicle V_x . In the state vector, V_y denotes the lateral velocity, V_x denotes the longitudinal velocity and ϕ denotes the yaw angle. The vehicle model refers to a high-performance autonomous car characterized by the parameters listed below.

- $m = 275$ kg, the total vehicle mass;
- $I_z = 104.8$ Nms², the yaw moment of inertia of the vehicle;
- $l_f = 0.824$ m, the longitudinal distance from the center of gravity to the front wheels;
- $l_r = 0.702$ m, the longitudinal distance from the center of gravity to the rear wheels;
- $C_{\alpha f} = 44222$ N/rad, the cornering stiffness of the front tires;
- $C_{\alpha r} = 44222$ N/rad, the cornering stiffness of the rear tires.
- $A = 1.2$ m², Frontal area.
- $C_x = 1.03$, Drag coefficient.

2.4 Driveline dynamics

Generally, a lower level controller is implemented to calculate the throttle input, to track the desired acceleration determined by the MPC, which uses a simplified model of longitudinal vehicle dynamics. This simplified model is typically based on the assumptions that the torque converter in the vehicle is locked and that there is zero-slip between the tires and the road.

For this thesis, based on the same assumptions of a simplified longitudinal dynamics model, a first order dynamics with a time constant of $\tau = 0.5s$, for the driveline is used. Which provides the required engine torque to track the desired acceleration. So, the engine torque required to track the desired acceleration is first calculated. This calculation is described in this section. Once the required engine torque has been obtained, engine maps and nonlinear control techniques are used to calculate to the throttle input command that will provide the required torque. The part for throttle input calculation has not been discussed in this thesis, and the reader can refer to [32] for more information on this topic.

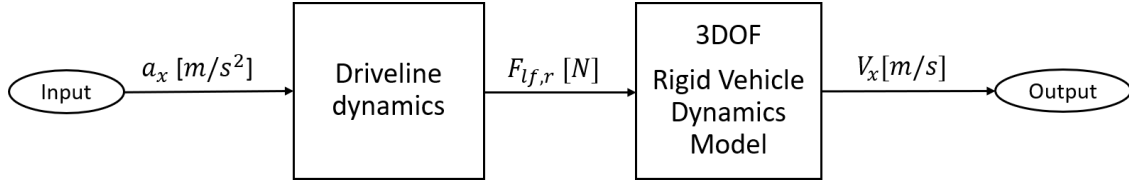


Figure 2.10: Driveline dynamics architecture

The required engine torque is given by:

$$T_{engine} = r_w(ma_x + 0.5\rho AC_x V_x^2) \quad (2.56)$$

The wheel torque for a given gear ratio i is given by:

$$T_{wheel} = T_{engine} \cdot i \quad (2.57)$$

The front and Rear wheel angular velocity is calculated:

$$J_{w,f}\dot{\omega}_f = T_w - T_b - r_w F_{l,f} \quad (2.58)$$

$$J_{w,r}\dot{\omega}_r = -T_b - r_w F_{l,r} \quad (2.59)$$

Wheel slip calculated based on Braking/Driving:

$$\sigma_i = \frac{r \omega_i - v_{x,i}}{v_{x,i}} \quad r \omega_i < v_{x,i} \quad \text{Braking} \quad (2.60)$$

$$\sigma_i = \frac{r \omega_i - v_{x,i}}{r \omega_i} \quad r \omega_i > v_{x,i} \quad \text{driving} \quad (2.61)$$

Friction coefficient as a function of longitudinal slip ratio is given by:

$$\mu(\sigma) = D \sin(C \tan^{-1}(B\sigma - E(B\sigma - \tan^{-1}(B\sigma)))) \quad (2.62)$$

Finally, the longitudinal force developed in the tires based on percent longitudinal slip is given by:

$$F_x = \mu(\sigma) F_z \quad (2.63)$$

This force is given as an input to the vehicle dynamics model to accelerate and reach the reference longitudinal speed V_{ref} , as depicted in Figure 2.10. The actual lower dynamics of model as shown below

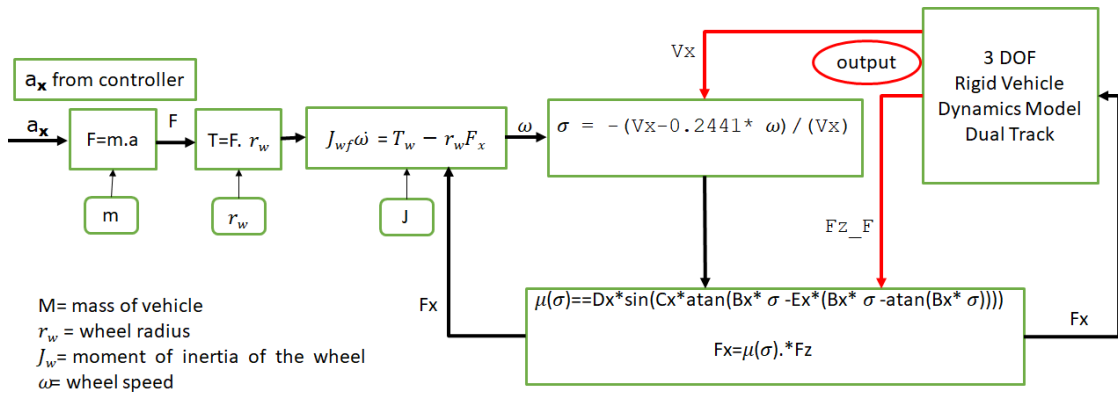


Figure 2.11: Lower dynamics architecture

Chapter 3

Control design

The aim of the controller is to safely achieve autonomous racing. The control strategy proposed here is considered in the global guidance architecture depicted in Figure 1.3. The architecture can be decomposed into three levels called Perception, Reference generation and Control:

- The Perception of the vehicle environment is of the utmost importance in the guidance architecture as it defines the environment in which the vehicle evolves. Its role is to provide the Reference generation with the necessary information.
- The Reference Generation provides reference signals. It allows the calculation of the geometric trajectory which defines the path to be followed as well as the reference speed profile. These two different reference signals calculated at this level are used by Control.
- The Control ensures the automated vehicle guidance along the generated trajectories providing the appropriate control signals, here the acceleration, the deceleration and the steering angle of the front wheel. Simultaneous longitudinal and lateral control is necessary to guarantee efficient vehicle guidance.

The architecture shown in Figure 3.1 highlights the interaction between the different blocks and present a combined controller for autonomous racing. Indeed, the lateral control is designed following a path tracking approach which helps to decouple the speed tracking and the vehicle positioning problems. However, the coupling of the longitudinal and lateral dynamics is handled by the MPC using the constraints

defined later in this section. The prediction model used here has two control inputs, i.e. the steering angle of the front wheel and the acceleration/deceleration. The steering angle is the variable of interest for lateral control and constitutes the optimization vector in the MPC problem. While, the applied acceleration/deceleration is used to track the reference velocity provide by the speed profile generator. Which is then used to calculate the required torque for the desired acceleration. In this way, MPC based lateral and longitudinal controller ensure the coupled path and speed tracking. Note that no active lateral stabilisation aspect is considered in the control design. In extreme lateral manoeuvres, vehicle stability may then be lost, e.g. when large steering manoeuvres are performed at high speed. In order to preserve vehicle lateral stability during guidance, the longitudinal reference speed should be adapted. To do so, a reference speed profile generator has been adopted, described in section 3.3.

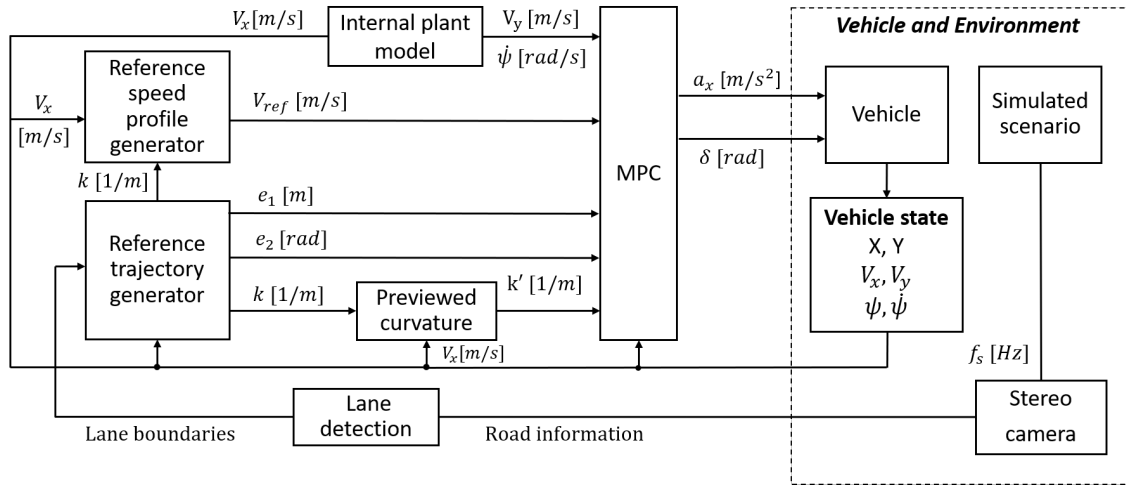


Figure 3.1: Detailed architecture of the control strategy

As mention in section 1.1, the overall system has been implemented in MATLAB and Simulink.

3.1 Lane detection

According to the the block scheme in Figure 3.1, in this section the stereo camera and lane detection block has been presented. In this work, the stereo camera is implemented in Simulink using the *Vision Detection Generator* block from *Automated Driving Toolbox*. Which generate vision detections from simulated scenarios at the intervals of 100ms. Therefore, simulated driving scenarios are used to simulate the environment and generate the synthetic data required for the control algorithm of the vision detection. In particular the detection of road lanes has been performed following a visual perception example included in the MATLAB documentation [44].

The vehicle position, velocities, yaw angle and yaw rate is feed to the sensor reader. A Scenario Reader block reads the actors and roads from the specified *Driving Scenario Designerr* file. The block outputs to Vision Detection Generator sensor blocks.

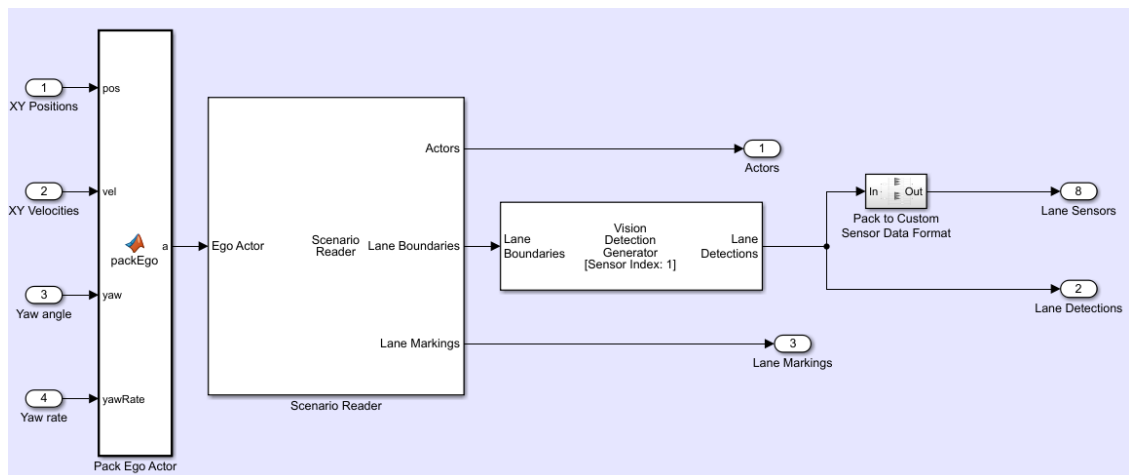


Figure 3.2: Sensor Simulation

Vision Detection Generator sensor blocks consist of a monocular camera sensor. Camera configuration information includes the intrinsic (Focal length and optical center of the camera) and extrinsic parameters (Orientation (pitch, yaw, and roll) and the camera location within the vehicle to define the camera orientation with respect to the vehicle's chassis) in the *Vision Detection Generator* block. The camera is mounted on top of the vehicle at a height of 1.5 meters above the ground and a pitch of 1 degree toward the ground. This information is later used to establish

camera extrinsics that define the position of the camera coordinate system with respect to the vehicle coordinate system. Focal length = [800, 800]; Optical center of the camera = [320, 240];

In this thesis, monocular camera sensor uses the built-in *findParabolicLaneBoundaries* function has been used to fit the lane line model. This function uses RANSAC algorithm to find the lane line boundaries. As the function name suggests, the model created is a parabolic model that fits a set of boundary points and an approximate width. The selected boundary points correspond to inliers only if they fall into the boundary width. The final parabolic model has been obtained using a least-squares fit on the inlier points.

The function receives in input the candidate points in vehicle coordinate from the features extraction phase and it provides array of *parabolicLaneBoundary* objects for each model. The returned array includes the three coefficients [a b c] of the parabola, like a second-degree polynomial equation ax^2+bx+c , and in addition the strength, the type, and the minimum and maximum x positions of the computed boundary. The last three parameters are used to reject some curves that could be invalid using heuristics. For example, in order to reject short boundaries, the difference between the minimum and maximum x positions has been compared with a specific threshold, if the minimum threshold is not reached, the found boundaries are rejected; or, to reject weak lines, the value of the strength has to be higher than another threshold set ad hoc.

3.2 Reference trajectory generation

The trajectory generation phase consists to find the trajectory and compute its curvature based on the information of the lane line model coming from the previous step. This phase refers to the problem of trajectory planning, also called motion planning, in automotive context, that has the purpose to find a trajectory feasible for the vehicle, and safe and comfortable for the passenger.

The motion planning for an autonomous vehicle is based on the same theory handled in robotics area. In fact, as in the field of robotics, it is necessary to provide and distinguish some definitions such as path and trajectory, and global and local planning.

Firstly, it is significant to give the definitions of path and trajectory and underline

that they have two different meanings:

- *Path* is the pure geometric description of motion;
- *Trajectory* is the merge of the path and the time laws (velocities and accelerations) required to follow the path.

The other significant definitions are global and local planning:

- *Global planning* means the generation of the path or trajectory knowing the entire environment and its information such as the position of the obstacle and the lane boundaries;
- *Local planning* means, instead, the computation of the path according to sensor data that represent local environment information.

In this thesis, for the sake of simplicity, no strict distinction has been adopted to distinguish path and trajectory when needed.

Moreover, the indication of the trajectory (or similarly path) is defined as a local path as mention in the previous definitions.

The trajectory computed for this work consists of the center line of the lane. It is computed like the average between the left line of the lane and the right ones.

3.2.1 Trajectory curvature computation

The controller of the lane keeping needs to receive the curvature of the trajectory like input to perform the control action on the steering angle.

“*The curvature of a curve parametrized by its arc length is the rate of change of direction of the tangent vector [45]*”.

Considering a curve $\alpha(s)$, where s is the arc length and the tangential angle ϕ , computed counterclockwise from the x-axis to the tangent $T = \alpha'(s)$, as shown in Figure 3.3, the curvature κ of α is defined, following the definition, as:

$$\kappa = \frac{d\phi}{ds} \tag{3.1}$$

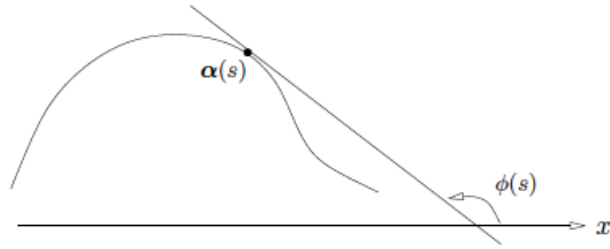


Figure 3.3: Curve α and tangential angle ϕ

The curvature can be also defined as the value of the turning of the tangent $T(s)$ along the direction of the normal $N(s)$, that is:

$$\kappa = T' \cdot N \tag{3.2}$$

It is easily to derive the first definition 3.1 from the second 3.2 (Figure 3.4), as follows:

$$\kappa = T' \cdot N = \frac{dT}{ds} \cdot N = \lim_{\Delta s \rightarrow 0} \frac{T(s + \Delta s) - T(s)}{\Delta s} \cdot N = \lim_{\Delta s \rightarrow 0} \frac{\Delta\phi \cdot \|T\|}{\Delta s} = \frac{d\phi}{ds} \tag{3.3}$$

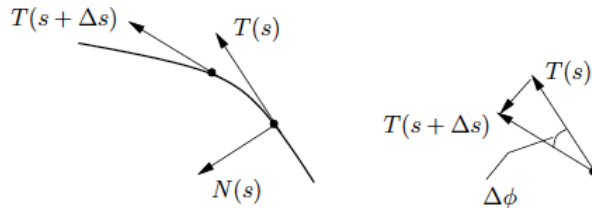


Figure 3.4: Demonstration that the definition 3.1 can be derived from the definition 3.2

To perform the measure of how sharply the curve bends, the absolute curvature of the curve at a point has been computed and it consists of the absolute value of the curvature $|\kappa|$.

A small absolute curvature corresponds to curves with a slight bend or almost straight lines. Curves with left bend have positive curvature, while a negative curvature refers to curves with right bend.

With the second definition 3.2 it is possible defined that the curvature of a circle is the inverse of its radius everywhere. For this reason, the radius of curvature R has been identified as the inverse of the absolute value of the curvature κ of the curve at a point.

$$R = \frac{1}{|\kappa|} \quad (3.4)$$

The circle with radius equal to the curvature radius R , when $\kappa \neq 0$, and positioning at the center of curvature is called *osculating circle*, as shown in Figure 3.5. It allows to approximate the curve locally up to the second order.

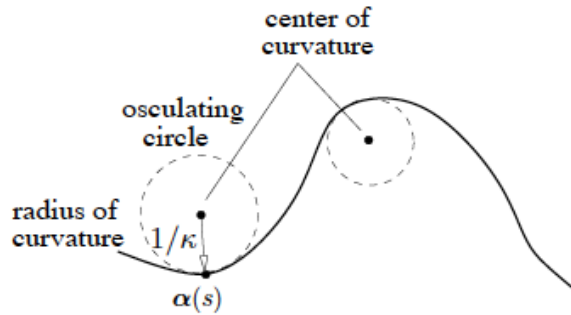


Figure 3.5: Osculating circle and radius of curvature

The curvature can be expressed in terms of the first and second derivatives of the curve α for simplicity in the computation, by the following formula:

$$\kappa = \frac{|\alpha''|}{[1 + (\alpha')^2]^{\frac{3}{2}}} \quad (3.5)$$

In order to compute the curvature in this thesis work, the *Geom2d* toolbox in MATLAB has been used. This toolbox provides the *polynomialCurveCurvature* function

that allows to compute the local curvature at specific point of a polynomial curve. It receives in input the curve in parametric form $x = x(t)$ and $y = y(t)$ and the point in which the curvature has to be evaluate.

The function *polynomialCurveCurvature* computes the curvature following the formula 3.5 that becomes:

$$\kappa = \frac{|x'y'' - x''y'|}{[(x')^2 + (y')^2]^{\frac{3}{2}}} \quad (3.6)$$

3.2.2 Computation of vehicle model dynamic parameters

The last phase of the lane detection algorithm refers to the computation of vehicle model dynamic parameters. These values are necessary in order to achieve the goal of the control stage for the lane keeping. The controller has to minimize the values of lateral deviation and relative yaw angle in order to compute the optimal steering angle.

Lateral deviation and relative yaw angle are defined as follow:

- *Lateral deviation* is the distance of the center of mass of the vehicle from the center line of the lane;
- *Relative yaw angle* is the orientation error of the vehicle with respect to the road.

These parameters are computed geometrically after a 2D reconstruction of the road (Figure 3.6): the lateral deviation is considered the distance between the camera mounted at the center of the vehicle that is become the origin of the new reference frame created by *monoCamera* object, and the center line computed in the previous phase; while, the relative yaw angle is identified as the angle between the vector of the longitudinal velocity and the tangent to the center line. With the information about the lane line model, the function performs a reconstruction of the road in order to computes the center line of the lane and the relative curvature, as specified in the previous section. Based on the computed trajectory, the lateral deviation and the relative yaw angle of the vehicle has been calculated as described in this section. Figure 3.7 shows an example of the plot in MATLAB about these computations.

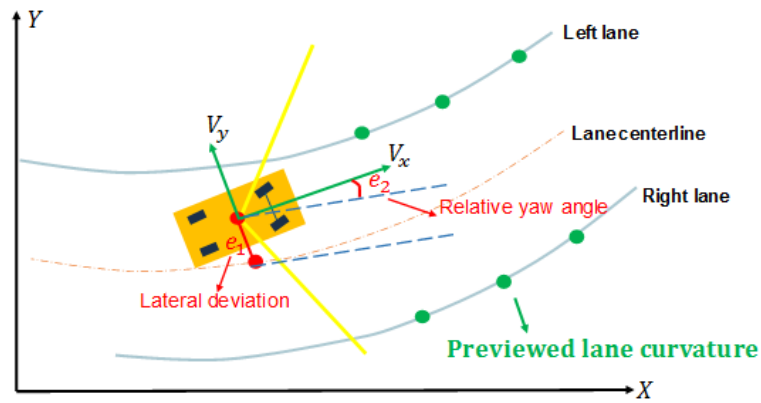


Figure 3.6: Definition of lateral deviation and relative yaw angle with respect the center line of the lane

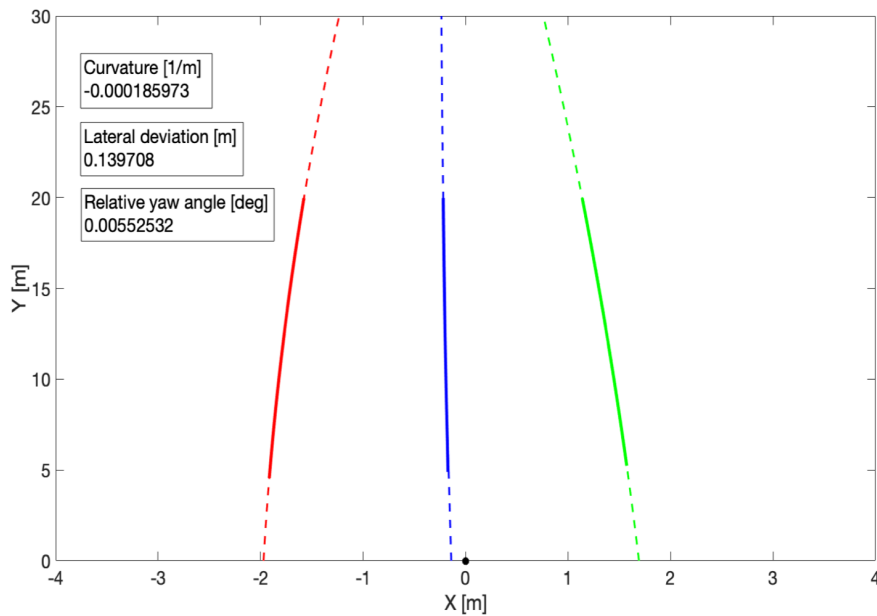


Figure 3.7: Center line, curvature, lateral deviation and relative yaw angle computation

3.3 Reference speed profile generation

The following subsections are devoted to determine the reference speed profile, two different criteria are considered here, which are available in literature. First one is based on the geometry of the road and the second one is based on the lateral comfort

of the vehicle. So, maximum admissible longitudinal speed is estimated based on the road information and the speed for lateral comfort is calculated based on the information about the desired lateral acceleration. Both of them are exploited to calculate the reference speed profile by the speed profile generator.

Road information criteria: the performance of the path-following depends on the speed with which this following is done. The cruise speed is also important for the stability of the vehicle on the road. In fact, no controller can ensure the path-following if the cruise speed is excessive. Thus, the speed of the vehicle should be reduced when approaching a bend. This adaptation of the cruise speed depends on the difficulty to cross the bend. There are several systems designed by automakers for assisting driver when approaching a bend, like those developed by Daimler-Chrysler defining the maximum admissible speed based on the curvature of the road:

$$V_{max} = \sqrt{\frac{g\mu}{\kappa}} \quad (3.7)$$

where g , μ and κ are respectively the gravity, the friction coefficient and the road curvature. The description given by the model (3.7) is incomplete and may be inappropriate to determine the maximum admissible speed in some situations. Indeed, the only parameter considered in this model is the road curvature. However, other characteristics of the road can be considered. For this reason, more sophisticated models are proposed. The National Highway Traffic Safety Administration (NHTSA) recommends for the calculation of the maximum entry speed in bends the following model:

$$V_{max} = \sqrt{\frac{g}{\kappa} \left(\frac{\phi_r + \mu}{1 - \phi_r \mu} \right)} \quad (3.8)$$

where ϕ_r is the road camber angle.

Then, the acceleration a that should be applied to bring the speed of the vehicle to the maximum admissible speed given by (3.8) should be less than:

$$a_{max} = \sqrt{\frac{V^2 - V_{max}^2}{2(d - t_r V)}} \quad (3.9)$$

where V is the current vehicle speed, d distance to the summit of the bend and t_r the time-delay due to driver reaction. The purely geometric models (3.7) and (3.8) can be evaluated in real-time and can be used in a predictive way as the road data are already employed in the MPC strategy. Notice that these criteria do not handle the vehicle lateral dynamics. Thus, in our work these criteria are combined with other indicators on the lateral stability presented in the following section. For lateral stability of the vehicle an additional condition is applied to improve the lateral motion. So, a desired longitudinal acceleration is calculated from physical limitation in braking with cornering.

$$a_x = \frac{\sqrt{(\mu gm)^2 - \sum(F_y)^2}}{m} \quad (3.10)$$

$$\sqrt{F_x^2 + F_y^2} < \mu F_z \quad (3.11)$$

In this way, a constrain on the longitudinal acceleration is imposed using the Kamm inequality, which keeps the forces developed in the tires within the physical limitations of the tire-road friction. Where, F_y can be either estimated or it can be measured using recently developed technology like smart tires or load sensing bearings to compute the a_x in real time.

The information on lateral dynamics is of capital importance as it helps to determine loss of control and help to preserve the lateral stability[46]. In this work, following criteria is used, which gives the β_{limit} :

$$\beta_{limit} < 10^\circ - 7^\circ \frac{(V_x)^2}{(40m/s)^2} \quad (3.12)$$

where, β is the sideslip angle of the vehicle and V_x is the vehicle speed.

The Reference Generation provides the lateral deviation and relative yaw angle to be minimized by the vehicle and a speed profile taking legal speed limits and vehicle comfort into account.

3.4 Model Predictive Control

In this section, theory behind Model Predictive Control will be explored together with the derivation of the Adaptive MPC, used to control the vehicle.

The aim of this thesis is to design a controller that allows autonomous driving. We decided to use Model Predictive Control, due to its abilities to work with constraints both on the states and the control signals. This is crucial for the control of a vehicle since it is constrained not only by mechanics of the vehicle but also by the environment. For example, a vehicle should not exceed the speed limits or drive too close to other vehicles.

3.4.1 Overview of MPC

Model Predictive Control (MPC) is an advanced control method that works in discrete time. From a set of state values, and with respect to a model, it optimizes a problem around an objective and gives a sequence of control signals as outputs. The first set of control values are then used as inputs to the system plant, and after a short period, set as the system time step, the new state values are measured and the process is repeated. In this section we will shortly describe the history of MPC and give some basic examples of its structure and the theory behind it.

The beginning of MPC was at Shell Oil Company in 1979 where an idea named as "Dynamic Matrix Control" was presented by Cutler and Ramaker [47]. DMC was the first type of predictive control that could be applied in industry. The idea was to handle multi variable control systems without any constraints and predict future values for linear systems. The idea that the algorithm would predict future plant behavior was discovered to lead to a less aggressive output and a smoother convergence to the target set point. Throughout the 80s MPC was popular mainly in industries such as chemical plants and oil refineries [48], i.e. in slow processes where the computational time of the solvers would not be a problem. In the 90s the theory of MPC matured and with faster solvers and computers the algorithm was now feasible for faster, more demanding systems. Today MPC has many applications, and as we will demonstrate in this thesis, one of them is in autonomous driving.

According to Qin and Badgwell [49], the overall objectives of a MPC controller are:

1. Prevent that input and output constraints are violated;
2. Optimize some output variables, while others outputs are kept in a specified ranges;
3. Prevent that the input variables have excessive movement;
4. Control the major number of process variables when a sensor or actuator is down or is not available.

Three critical steps affect the process of a MPC controller: prediction model, optimization solution and feedback correction.

A general architecture of a Model Predictive Control used for autonomous driving vehicle is given by Figure 3.8.

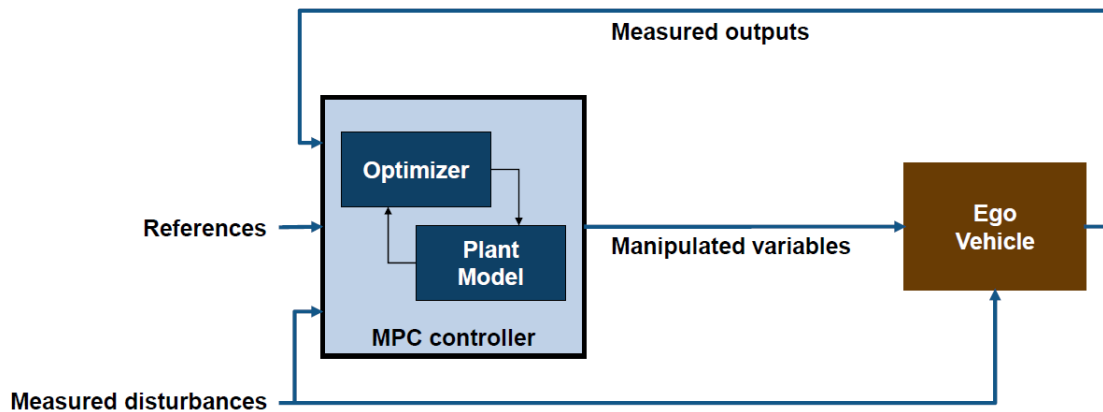


Figure 3.8: Block diagram for Model Predictive Control

MPC controller has two main functional blocks: the optimizer and the vehicle model. The dynamic optimizer allows to find the optimal input that gives the minimum value of the cost function taking into account all the constraints. The vehicle and the plant model refers to the 3DoF rigid vehicle model and a linearized state space model, described in the section 2.3. Generally, a non linear model is used for the validation of the controller, while the plant model used for the MPC is a linearized version of the actual plant.

The MPC controller provides the optimal output to send to a plant based on a finite horizon using an iterative approach. Its main goal is to calculate a sequence of *control moves*, that consist of manipulated input changes, so that the predicted output moves to the set point in an optimal manner.

Referring to Figure 3.9, y is the actual output, \hat{y} is the predicted output and u consists of the manipulated input. At the current sampling time k , the initial value of the plant state is known and the MPC computes a set of M values of the input $u(k+i-1)$, $i = 1, 2, \dots, M$, where M is called *control horizon*. This set refers to the current input $u(k)$ and to $(M - 1)$ prediction inputs, and it is held constant after the M control moves. The inputs are computed so that a set of N predicted outputs $\hat{y}(k + i)$, $i = 1, 2, \dots, N$ reaches the set point in optimal manner. N is called *prediction horizon* and consists of the number of future steps to look ahead [51].

When we are driving we never look straight down at the road, but farther ahead. The reason is of course so that we can plan our driving. When a sharp turn approaches we need to brake ahead of time. A driver always looks far enough to ensure safe driving, so called minimum braking distance, in case of an unexpected obstacle on the road. This should also apply in control. In Model predictive control there is a finite prediction horizon set for each optimization, i.e., how far the controller looks into the future. To decide the length of the horizon we can again draw an analogy to human driving. While driving at high speeds you need a longer prediction horizon since the minimum breaking distance is also longer. The prediction horizon must be long enough such that distance between the two cars are larger than the minimum braking distance. A longer horizon is usually ideal but is often limited by sensor limitations. The computational complexity also increases

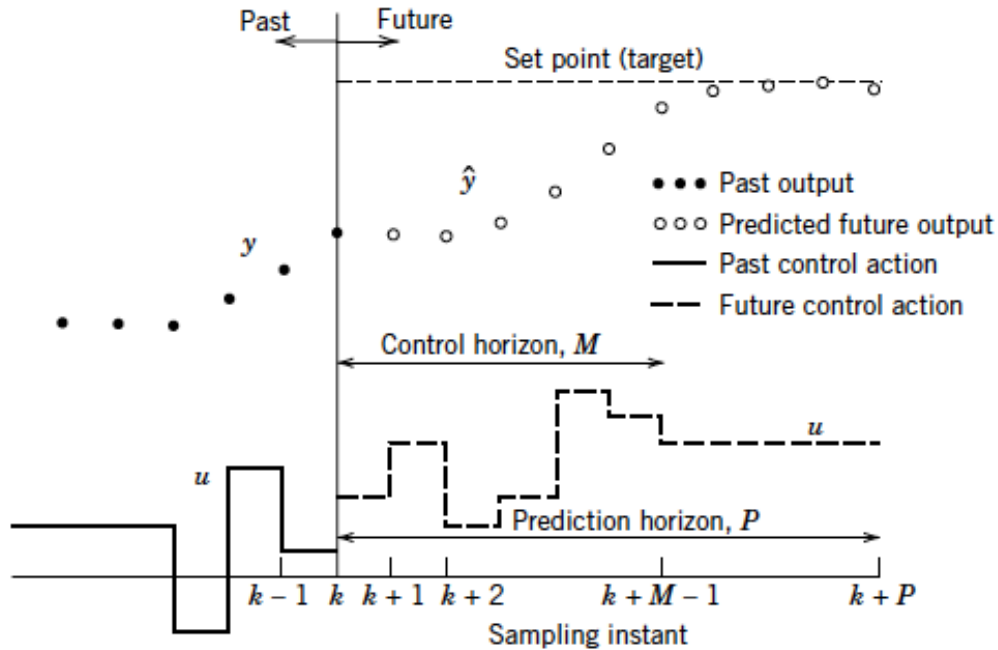


Figure 3.9: Basic concept for Model Predictive Control

for longer horizons, mainly for complex non-linear systems. So, the values of control horizon M is usually kept lower than the prediction horizon N as the controller apply only first control step and solves the optimization problem again. In practical situations, only the first value of the whole set of M values is implemented as the input of the system because the model of the process is simplified and inaccurate. Moreover, this set can add disturbances or noises in the process that could produce an error between the actual output and the predicted one.

For this reason, the plant state has to be measured again to be adopted as the initial state for the next step. The re-measurement of the information state is reported with a feedback to the dynamic optimizer of the MPC controller and adds robustness to the control [50]. When the plant state is re-sampled, the whole process computes again the calculations starting from the new current state. The window of the prediction horizon shifts forward at every time step. This is the reason why the Model Predictive Control is also called *Receding Horizon Control*.

3.4.2 MPC problem formulation

The MPC controller implemented in this thesis is based on the method of multiple-step optimization and feedback correction. Thanks to this method, the controller has good performances of control.

Lateral control deals with the actuation of the steering of the vehicle to keep it in the center of the lane and follow the curved road. It is modeled as a reference path tracking problem for the MPC with the objective of minimizing the lateral deviation e_1 and relative yaw angle e_2 . While, the longitudinal control deals with the actuation of the throttle/brake to control the longitudinal speed of the vehicle. It is modelled as a reference speed tracking problem, which is generated using the reference speed profile calculated using (3.12). Based on the reference velocity MPC computes the desired acceleration command to attain it. In other words, the objective of the MPC is to converge the speed of the vehicle to the desired reference speed. The inputs for the MPC are actual longitudinal velocity V_x , lateral deviation e_1 and relative yaw angle e_2 , which are the outputs of the actual plant model. i.e. 3DoF rigid vehicle model. Based on these three inputs the MPC solves the optimization problem as reference tracking. The reference variables are given by reference velocity V_{ref} , while e_1 and e_2 are set equal to zero. So, The goal of the MPC controller is to compute the optimal steering angle and throttle/brake command to perform the autonomous driving. In order to achieve this goal, the controller calculates the steering angle and throttle/brake by minimizing its cost function.

The description of the Adaptive MPC has been divided two parts:

- *Problem formulation* in which is explained how the MPC problem has been formulated;
- *Output prediction* in which is defined how the predicted output has been computed.

Problem formulation

The formulation of the MPC problem developed in this thesis starts defining a linear state-space model derived in section 2.3, which is represented as:

$$\begin{aligned}x(k+1) &= Ax(k) + B_u u(k) + B_d v(k) \\ y(k) &= Cx(k)\end{aligned}\tag{3.13}$$

Where:

- A is the state matrix;
- B_u and B_d are the input matrices corresponding to inputs u and v respectively;
- C is the output matrix.

Given the linear model defined in equation 3.13, the Model Predictive Control algorithm is implemented as solving the following optimization problem at each time step:

$$\begin{aligned}\min_u J &= \sum_{j=1}^N \|y_p(k+j|k) - y_{ref}(k+j|k)\|_{Q_y} + \sum_{j=0}^{M-1} \|u(k+j|k)\|_{R_u} \\ s.t. \quad &x(k+j+1|k) = Ax(k+j|k) + B_u u(k+j|k) + B_d v(k+j|k) \\ &x(k|k) = x(k) \\ &y(k+j|k) = Cx(k+j|k) \\ &|u(k+j|k)| \leq u_{limit}\end{aligned}\tag{3.14}$$

Where u is the manipulated variable. Q_y and R_u are weights for outputs and manipulated variables respectively. This optimization problem refers to find the value of input u that minimizes the sum of the weighted norms of the error between the predicted output vector y_p and the reference vector for those states y_{ref} and the input vector u for a defined prediction horizon N and control horizon M . The predicted output y has to satisfy the linear model, while the value of u should not exceed a specified limit u_{limit} .

The state vector y is given by:

$$\begin{bmatrix} V_x & e_1 & e_2 \end{bmatrix}^T$$

While, the state vector y_{ref} is given by:

$$\begin{bmatrix} V_{ref} & 0 & 0 \end{bmatrix}^T$$

V_x is directly taken from the vehicle dynamics block as an output while e_1 and e_2 are taken from the reference trajectory block. These three states are sent as feedback to the MPC controller in order to correct the control variables in the future step time with respect to the reference states.

The weighted norm of the vector $y = \begin{bmatrix} y_1 & y_2 & y_3 \end{bmatrix}^T$ corresponds to:

$$\|y(k+j|k)\|_{Q_y} = \begin{bmatrix} y_1 & y_2 & y_3 \end{bmatrix} \begin{bmatrix} q_{11} & 0 & 0 \\ 0 & q_{22} & 0 \\ 0 & 0 & q_{33} \end{bmatrix} \begin{bmatrix} y_1 \\ y_2 \\ y_3 \end{bmatrix} \quad (3.15)$$

where the weights q_{11} , q_{22} and q_{33} are tuned to provide the needed damping on the corresponding output. The same definition is applied to the weighted norm of u given by:

$$\|u(k+j|k)\|_{R_u} = \begin{bmatrix} u_1 & u_2 \end{bmatrix} \begin{bmatrix} r_{11} & 0 \\ 0 & r_{22} \end{bmatrix} \begin{bmatrix} u_1 \\ u_2 \end{bmatrix} \quad (3.16)$$

Output prediction

The values of the predicted output $y(k+j|k)$, $j = 1, 2, \dots, N$, where N is the prediction horizon, have been computed using the linear state-space model described by the formula 3.13.

In particular, in order to make the computation, the following values have to be known:

- Present output measurement $y(k|k) = y(k)$;
- Applied input $u(k|k) = u(k)$;
- Entire set of predicted input values $v(k+j|k)$, $j = 0, 1, 2, \dots, N$.

If the prediction state is defined as follows:

$$\begin{aligned}
 x(k+1|k) &= Ax(k) + B_u u(k|k) + B_d v(k|k) \\
 x(k+2|k) &= Ax(k+1|k) + B_u u(k+1|k) + B_d v(k+1|k) = \\
 &= A^2 x(k) + AB_u u(k|k) + AB_d v(k|k) + B_u u(k+1|k) + B_d v(k+1|k) \\
 &\quad \vdots \\
 x(k+N|k) &= Ax(k+N-1|k) + B_u u(k+N-1|k) + B_d v(k+N-1|k) = \\
 &= A^N x(k) + A^{N-1} B_u u(k|k) + A^{N-1} B_d v(k|k) + A^{N-2} B_u u(k+1|k) + \\
 &A^{N-2} B_d v(k+1|k) + \dots + B_u u(k+N-1|k) + B_d v(k+N-1|k)
 \end{aligned} \tag{3.17}$$

The prediction output can be identified by the following equations:

$$\begin{aligned}
 y(k|k) &= Cx(k) \\
 y(k+1|k) &= Cx(k+1|k) \\
 y(k+2|k) &= Cx(k+2|k) \\
 &\vdots \\
 y(k+N|k) &= Cx(k+N|k)
 \end{aligned} \tag{3.18}$$

Using the equations 3.17 and 3.18, it is possible to express the predicted outputs $y(k+1|k), \dots, y(k+N|k)$ as a function of the predicted inputs $u(k|k), \dots, u(k+N-1|k)$, noted that the other signals are assumed to be known as stated above.

In order to make the relation between the equations 3.17 and 3.18 clearer, the prediction output of the future can be defined as follows:

$$Z(k) = Gx(k) + HU(k) + EV(k) \tag{3.19}$$

Where:

- $Z(k)$ is the augmented vector of the predicted outputs;
- $U(k)$ is the augmented vector of the computed future inputs;
- $V(k)$ is the augmented vector of the predicted disturbances.

These vectors are obtained by the chaining of the input and the output vectors in the present time until the future N vectors ($N - 1$ vectors for the input u and v), and they are defined as follows:

$$Z(k) \equiv \begin{bmatrix} z(k|k) \\ z(k+1|k) \\ \vdots \\ z(k+N|k) \end{bmatrix}; U(k) \equiv \begin{bmatrix} u(k|k) \\ u(k+1|k) \\ \vdots \\ u(k+N-1|k) \end{bmatrix} \text{ and } V(k) \equiv \begin{bmatrix} v(k|k) \\ v(k+1|k) \\ \vdots \\ v(k+N|k) \end{bmatrix}$$

The matrices G, H and E are determined in the following way:

$$G = \begin{bmatrix} C \\ CA \\ CA^2 \\ \vdots \\ CA^N \end{bmatrix}; H = \begin{bmatrix} 0 & 0 & 0 & \dots & 0 \\ CB_1 & 0 & 0 & \dots & 0 \\ CAB_1 & CB_1 & 0 & \dots & 0 \\ \vdots & \vdots & \vdots & \vdots & \vdots \\ CA^{N-1}B_1 & CA^{N-2}B_1 & CA^{N-3}B_1 & \dots & CB_1 \end{bmatrix} \text{ and}$$

$$E = \begin{bmatrix} 0 & 0 & 0 & \dots & 0 \\ CB_2 & 0 & 0 & \dots & 0 \\ CAB_2 & CB_2 & 0 & \dots & 0 \\ \vdots & \vdots & \vdots & \vdots & \vdots \\ CA^{N-1}B_2 & CA^{N-2}B_2 & CA^{N-3}B_2 & \dots & CB_2 \end{bmatrix}$$

As mentioned before, the proposed control strategy maximizes the longitudinal speed while remaining in constrained speed range and without exceeding the adherence condition. At the same time, it eliminates the path error between the actual location and the desired path in terms of lateral deviation and desired yaw angle, assuring the handling stability during the motion.

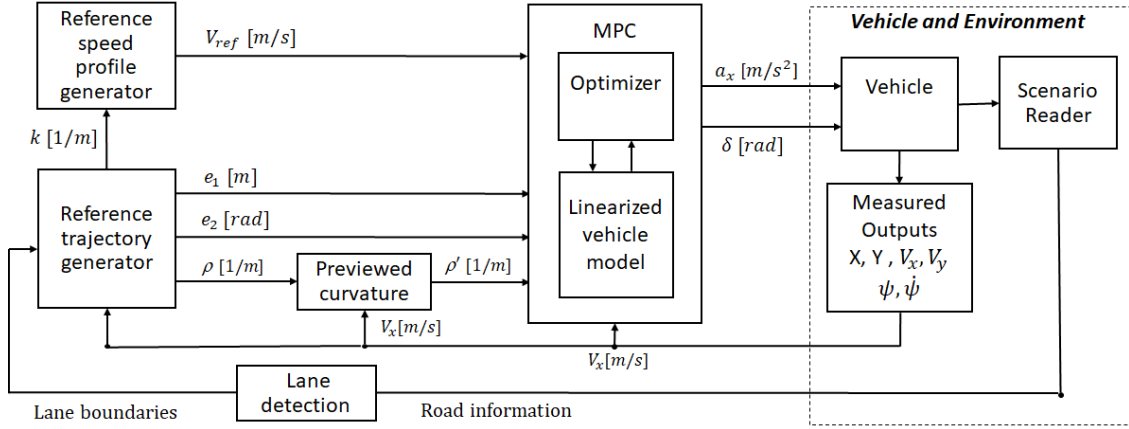


Figure 3.10: Architecture of MPC Controller

3.5 Decoupled Controller

The conventional theory on decoupling control describes how a system with multiple inputs and outputs (MIMO) can have a controller that isolates the inputs and outputs so that one input affects only one output instead of multiple. The act of doing so is called decoupling. In vehicle control, the vehicle models have coupled kinematic and dynamics which means that lateral and longitudinal dynamics may affect each other.

Decoupled control of a vehicle means that the longitudinal and lateral dynamics of the vehicle are handled separately by two different controllers. In [52], the authors state that the dynamical forces of a vehicle must be kept low in order to have lateral and longitudinal dynamics controlled separately. This means that the decoupled control may be limited by the dynamics of the vehicle.

In practice, a decoupled control strategy uses two different control approaches for the lateral and longitudinal dynamics. Generally, the longitudinal control will be first to optimize the acceleration and speed of the vehicle before it feeds the lateral controller with the current speed of the vehicle. The lateral controller then uses the information about the speed in order to output a suitable steering angle [53]. A simplified drawing of the decoupled control system is shown in Figure 3.11.

In this thesis, the two decoupled control strategy MPC-PID Controller and PID Controller are used. In MPC-PID controller, PID-controller for the longitudinal controller and an MPC controller for the lateral control. To handle longitudinal constraints, the PID-controller will be subject to control input saturation to avoid too large vehicle accelerations. In second controller, PID Stanley controller are used for longitudinal and lateral control.

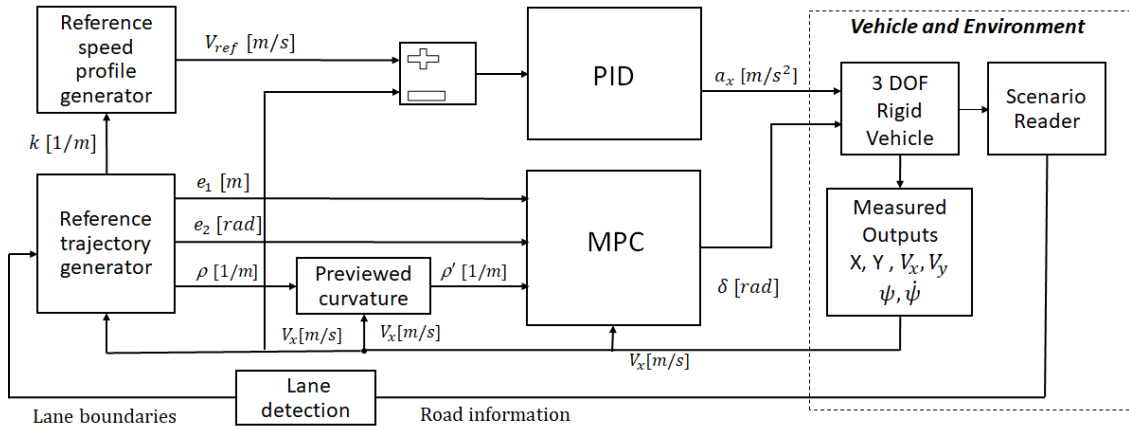


Figure 3.11: Architecture of MPC-PID controller

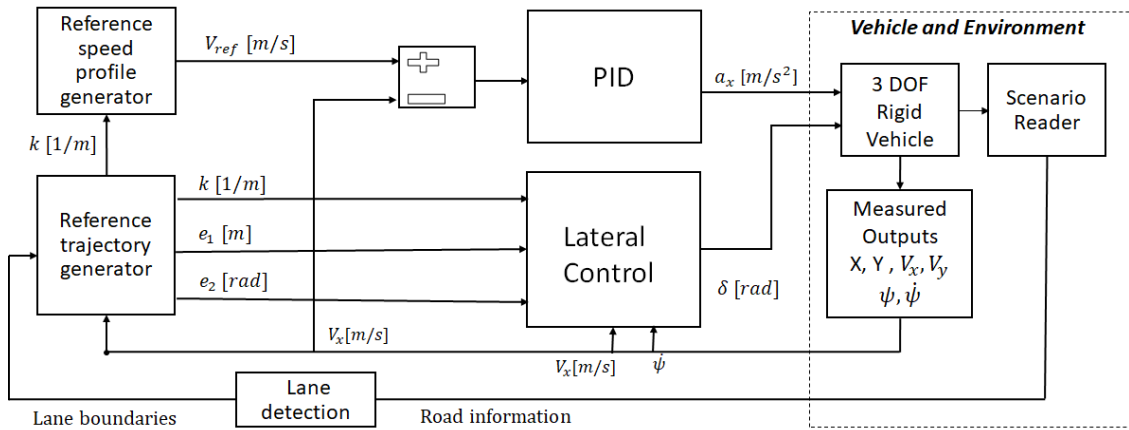


Figure 3.12: Architecture of PID-Stanley controller

3.5.1 PID Controller

Proportional-Integral-Derivative controller, known as PID, is a widely used technique in feedback control applications. The PID controller, despite its simplicity, is a potent controller and have been used in applications where a vehicle is supposed to track a specified path. PID output depends on an input error signal and three tunable gains changing the response of the system. A major advantage is that it reduces the steady state error through the integral action; in addition, derivative gain allows predicting future actions. 3.20 shows the general formula for a discrete time PID controller using the forward Euler method.

$$u_z = K_p + K_i \frac{T_s}{z-1} + K_d \frac{z-1}{T_s z} \quad (3.20)$$

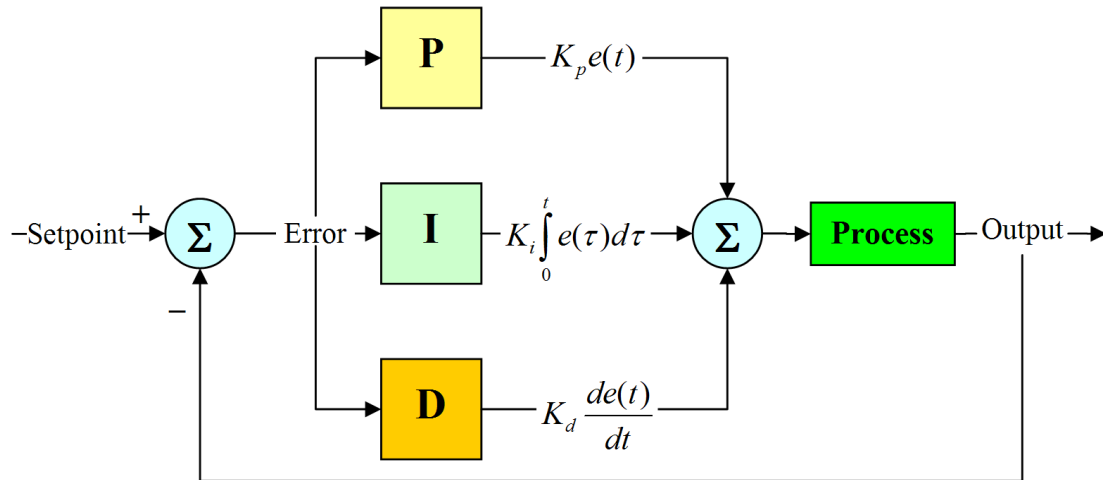


Figure 3.13: PID feedback loop

where u_z is the control output and K_p , K_i and K_d represent the proportional, integral, and derivative gains, respectively; T_s corresponds to system sample time. PID controllers have been used for different automated driving longitudinal applications and appear as a practical solution for ACC applications where control signals can be modified according to the speed error and selecting the proper gains.

3.5.2 Stanley Controller

Gabriel M. Hoffmann [54] presents the Stanley controlling method, developed and used by Stanford Racing Team in DARPA Grand Challenge 2005. Asymptotic stability is proven for the controller using the kinematic equations of motion and the controller is extended with dynamic models for the pneumatic tires and the servo actuated steering wheel. Stanley controller have shown great potential for lateral control off road vehicles in rough environments. The controller uses the lateral error, orientation error and the velocity of the vehicle as input.

The controller on standard form can be written as

$$\delta = e_2 + \frac{\kappa e_1}{V_x} \quad (3.21)$$

where κ is a gain variable, V_x is the velocity of the vehicle, e_1 is the lateral error and e_2 the orientation error of the vehicle.

The control method uses a similar structure to the PID controller, but Stanley is a MISO system and uses the lateral error, orientation error and velocity as input parameters. Stanley uses the nonlinear feedback function arctan, for which exponential convergence can be shown [39]. The controller structure is depicted in Figure 3.14

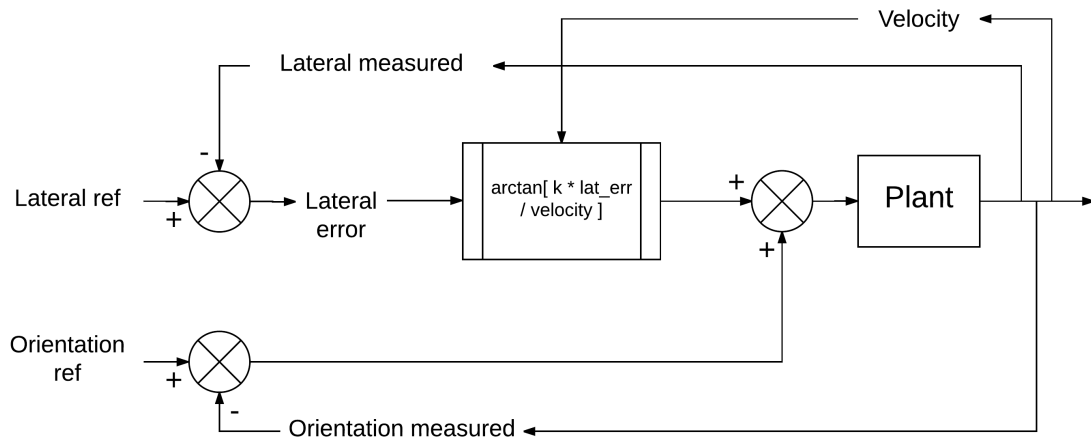


Figure 3.14: Stanley controller

The basic Stanley controller has, only one gain, κ . This leaves the user with a limited possibility for adjusting and tuning. Therefore, it might not be optimal when

tuning the controller for a specific vehicle, as few gains will limit the controllers possibility for optimal performance. The controller performance can be improved significantly by adding additional parameters, extended controller formula, defined as[38]

$$\delta = e_2 - e_{ss} + \frac{\kappa e_1}{\kappa_{soft} + V_x} + \kappa_d(r_{mean} - r_{traj}) \quad (3.22)$$

$$e_2 = \Psi - \Psi_{des} \quad (3.23)$$

$$e_{ss} = \frac{m V_x r_{traj}}{C_y(1 + a/b)} \quad (3.24)$$

$$r_{traj} = \frac{V_x}{R} \quad (3.25)$$

where κ is a tuned gain and κ_{soft} is a tuned gain, permitting the control to be soft at low velocities. κ_d is a tuned gain which adjusts to what extent the subtraction of the measured yaw rate of the vehicle and the trajectory yaw rate will affect the control. The purpose of this term is to create an active damping as the velocity increases. κ_d is a tuned gain which adjusts to what extent previous steering angle will affect the control. This term will limit the issues in the steering, such as time delay and overshoot. e_1 is the lateral error, e_2 is the orientation error and e_{ss} is the steady state yaw. r_{mean} is the orientation of the vehicle and r_{traj} is the orientation of the nearest perpendicular trajectory.

Chapter 4

Results and discussions

In this chapter racing simulation are presented for different type of controller and later the simulation results are presented and discussed.

4.1 Setup

In order to implement the controller, a simulation environment has been developed in MATLAB. It consists of user-defined race track. We have considered racing scenarios represented in Figure 4.1 to validate the proposed control strategies.

4.1.1 Racetrack and The Car

The racetrack is the centerline of the track defined by the user as the racing road. It can be generated by fitting a spline to a set of waypoints. The track length is around 2555m and width is 6m. overall system has been implemented in MATLAB and Simulink and the racing scenarios are created using the *Driving scenario designer application* in the Automated driving toolbox.

In the figures below, the racetrack scenarios with their road curvature are represented. The racetrack scenario Figure 4.1 is characterized by a typical racetrack. The vehicle data are collected from SquadraCorse racing team, SquadraCorse is a

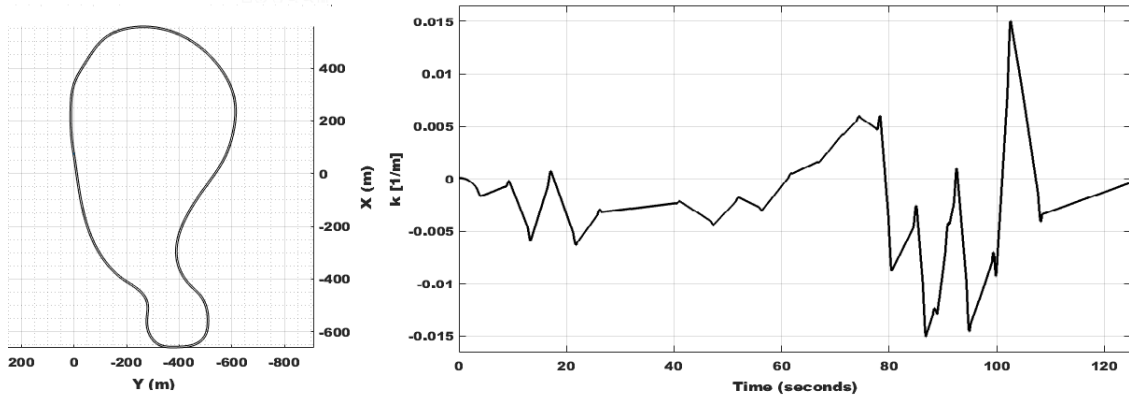


Figure 4.1: (a) Racetrack scenario (b) Detected road curvature k

student racing team of the Politecnico di Torino, the data as show below

- $m = 275$ kg, the total vehicle mass;
- $I_z = 104.8$ kgm^2 , the yaw moment of inertia of the vehicle;
- $l_f = 0.824$ m, the longitudinal distance from the center of gravity to the front wheels;
- $l_r = 0.702$ m, the longitudinal distance from the center of gravity to the rear wheels;
- $C_{\alpha_f} = 44222$ N/rad, the cornering stiffness of the front tires;
- $C_{\alpha_r} = 44222$ N/rad, the cornering stiffness of the rear tires.
- $A = 1.2$ m^2 , Frontal area.
- $C_x = 1.03$, Drag coefficient.

4.2 Results and discussion

In this section the results from the simulations are presented and discussed.

For validation purposes speed tracking, lateral deviation and steering angle is considered. It gives information about how much the vehicle deviates in the lateral direction from the center line of the lane and the latter how much the vehicle's yaw angle deviates from the desired yaw angle. i.e relative yaw angle. A lateral deviation limit value equal to ± 0.10 m is considered as acceptable. Similarly, the relative yaw angle should be limited to ± 0.10 rad. Lateral acceleration is limited using the formula in equation(3.11), which keeps it in the adherence limit of (± 9 m/s^2) as seen in GG plot.

4.2.1 Sensitivity Analysis of MPC

Sensitivity analysis is the study of how the uncertainty in the output of a mathematical model or system (numerical or otherwise) can be divided and allocated to different sources of uncertainty in its inputs. In this analysis, by adjusting Weights and constraints of Manipulated variable(MV) and Measured Output to improve model predictive controller performance.

A model predictive controller uses linear plant, disturbance, and noise models to estimate the controller state and predict future plant outputs. Using the predicted plant outputs, the controller solves a quadratic programming optimization problem to determine optimal manipulated variable adjustments.

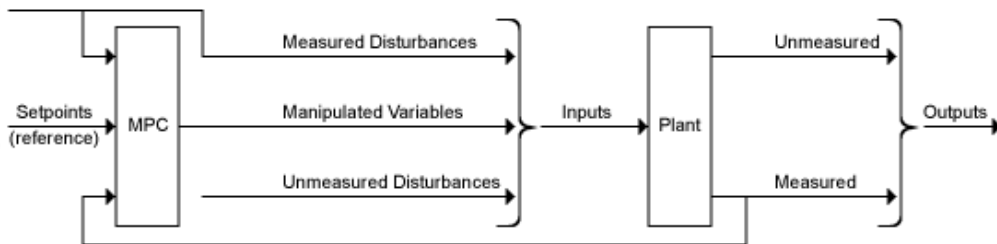


Figure 4.2: Basic workflow for designing traditional model predictive controllers

For this thesis, we have considered following variables

- Reference = Speed profile
- Manipulated variable(MV)= Acceleration and Steering Angle
- Measured Output(MO)= Lateral deviation, relative Yaw angle and Longitudinal velocity

4.2.2 Weights and Constraints

Constraints:it is possible to define maximum and minimum values for each one of the MV's and OV's, including their maximum down and up rates. This is a very important component when designing a controller for the MPC approach can deal with process constraints in an optimal fashion, so one may feel free to test and evaluate closed-loop responses with different constraints.

For this thesis, there is input constraints on manipulated variable to limit the maximum acceleration and steering angle.

Tune Weights for optimization: A model predictive controller design usually requires some tuning of the cost function weights. choose values for input and output weights according to their desired closed-loop response. If the system is multivariable, it is possible to set a tight control routine over a certain OV by tuning output weights, or if the controller is being too aggressive or too sluggish when dealing with MV's, tuning the input weights may turn to be a good option. Moreover, tuning weights is a quick way to choose between a more robust or faster response by managing the "Overall weight" (upper slide bar); one can designate values between 0 (more robust response) and 1.0 (faster response), being aware that overall weight's values close to one may destabilize the system depending on which values were set to prediction and control horizons.

in this thesis,there is weight constraints on manipulated variable, which is Robustness for acceleration and steering to minimize jerk (derivative of acceleration) and derivative of steering. and also on measured Output to minimize error against measured velocity and lateral deviation and yaw angle.

To improve model predictive controller performance, by adjusting Constraints and weights different simulation are executed as show in Figure 4.3 to get optimized result for MPC.

Constraints and Weights					
Acceleration	MV1	4	6	8	10
Steering Angle	MV2	15	20	25	30
Acceleration	Weights.MV1Rate	0.2	0.4	1	2
Steering Angle	Weights.MV2Rate	0.1	0.3	0.5	1
Longitudinal velocity	Weights.OV 1	1	2	3	4
lateral deviation	Weights.OV 2	0.1	0.5	1	2
Relative yaw angle	Weights.OV 3	0.1	0.2	0.3	0.4

Figure 4.3: MPC Constraints and Weights

Finally, we have selected the optimized parameters for MPC, which as show bwlow

- Sample Time= 0.1
- Prediction horizon = 10
- Control horizon = 2
- Acceleration(MV1) = 8
- Steering angle(MV2)= 15
- Acceleration(Weights.MV1Rate) = 0.4
- Steering angle(Weights.MV2Rate)= 0.1
- Logitudinal Velocity(Weights.OV1) = 3
- Lateral Velocity(Weights.O2) = 1
- Relative Yaw angle(Weights.OV3) = 0.1

4.2.3 Coupled Controller: MPC

For this thesis, we have considered The maximum longitudinal speed is $25m/s^2$ and lateral acceleration is $9 m/s^2$. The vehicle executes some maneuvers at Low speed with large curvature and some at high speed with very low curvature. In otherwords, the vehicle navigates within a very narrow turn at low speed then it accelerates to reacha high speed on a low curvature road. The longitudinal speed reference V_{ref} is accurately tracked by the car Figure 4.4. A maximum lateral deviation e_1 in Figure 4.5 equal to 0.15m is detected in regions with high curvature turns, while it assumes small values in the remaining part of the simulation ranging from ± 0.1 m. The error of the relative yaw angle e_2 in Figure 4.6 remains in the admissible range ranging from ± 0.10 rad. The value of the δ in Figure 4.7 varies between ± 1.5 degree to follow the center line of the lane. The GG diagram in Figure 4.13 confirms that the car is driving within the limits of adherence conditions.

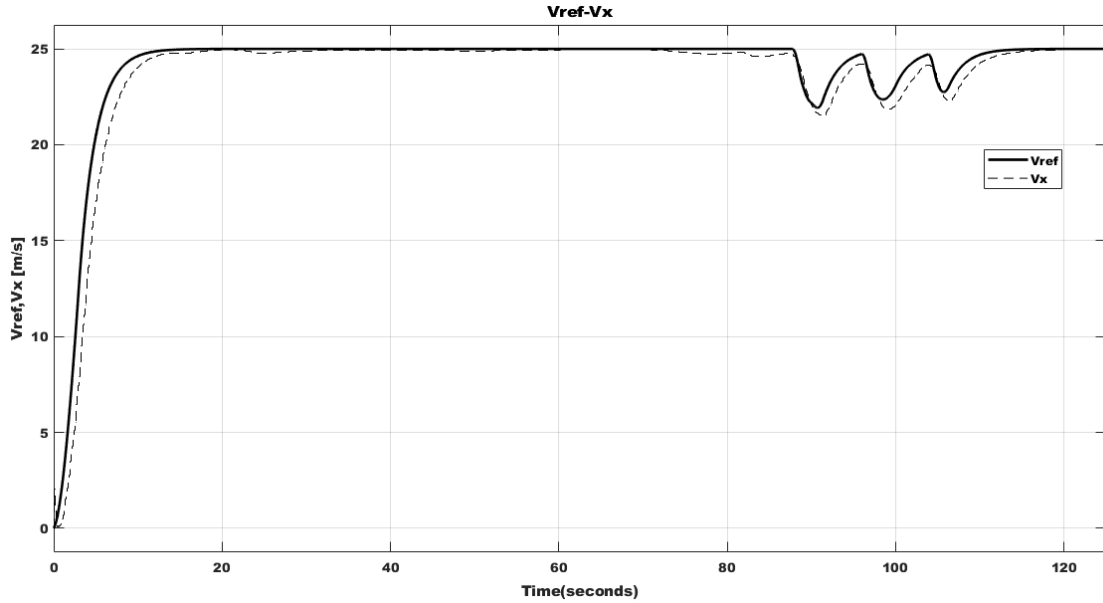


Figure 4.4: Measured vehicle's longitudinal speed V_x (dashed) vs. vehicle's longitudinal speed reference V_{ref} (solid)

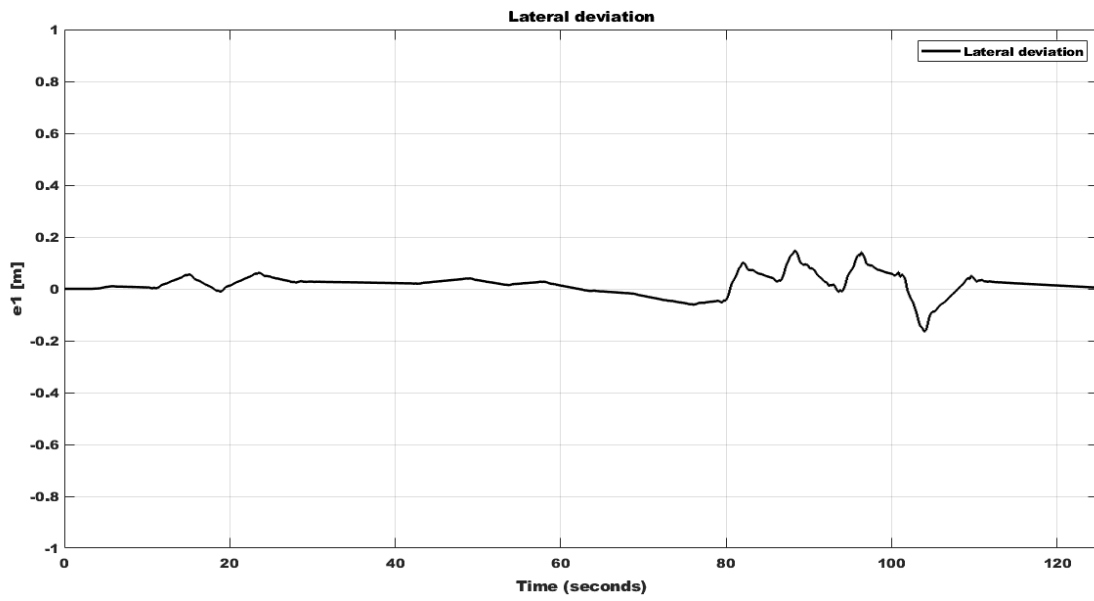


Figure 4.5: Lateral deviation e_1

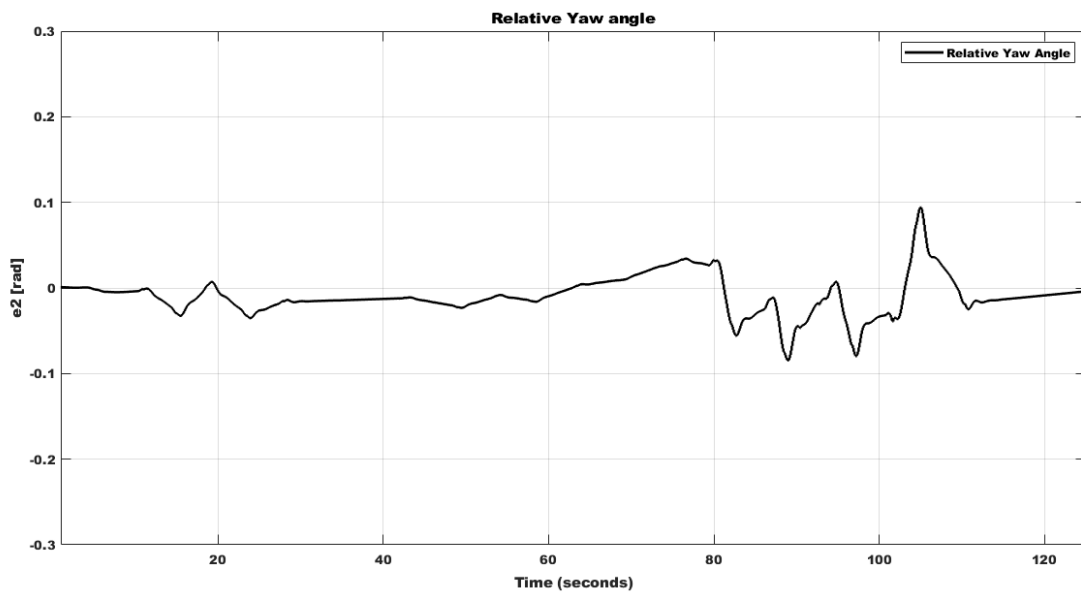


Figure 4.6: Relative yaw angle e_2

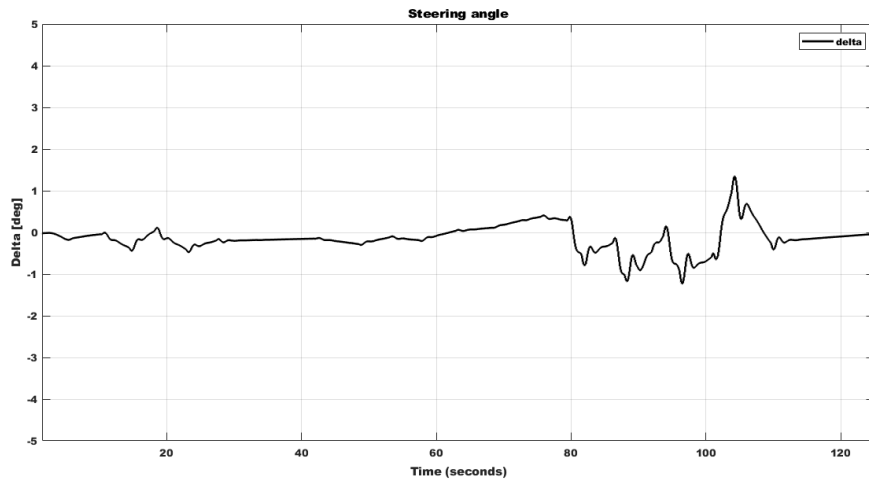


Figure 4.7: Front wheels steering angle command δ

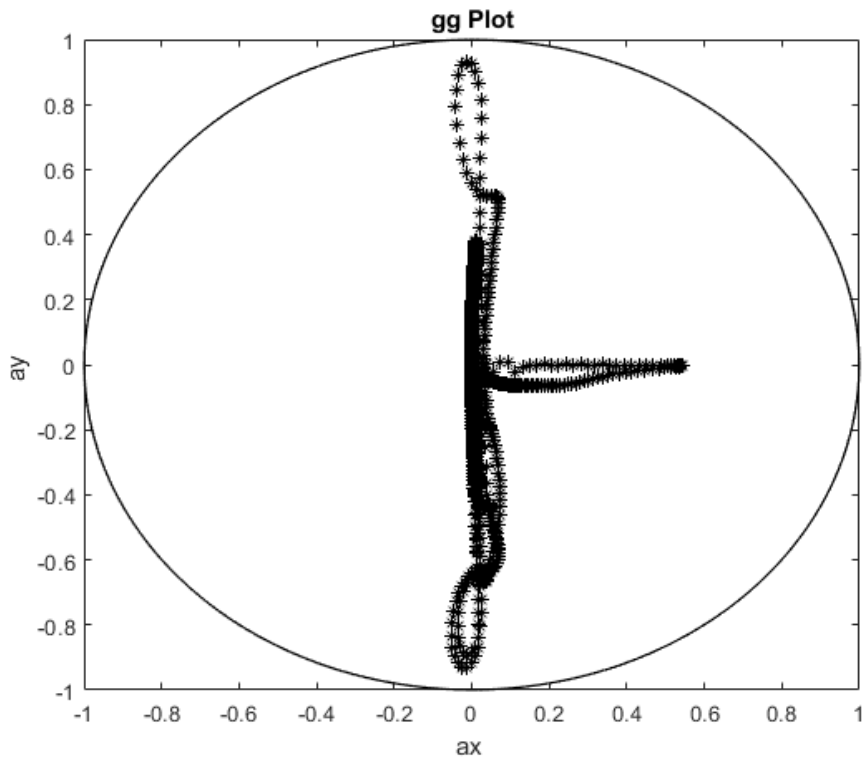


Figure 4.8: GG plot with the ellipse representing the adherence limits-MPC

4.2.4 Comparison with decoupled controller: MPC+PID and PID+P

In this section, the adaptive MPC is compared with decoupled controller MPC+PID and PID+P. Later, the results are compared and the advantages of the coupled lateral and longitudinal controller respect to the decoupled one are discussed.

The decoupled controller developed for autonomous racing uses a MPC/P for the lateral control, while for the longitudinal control a PID controller is used. Which tracks the reference velocity generated using only the road geometry and try to maximize it without any consideration of lateral stability. It can be seen that the

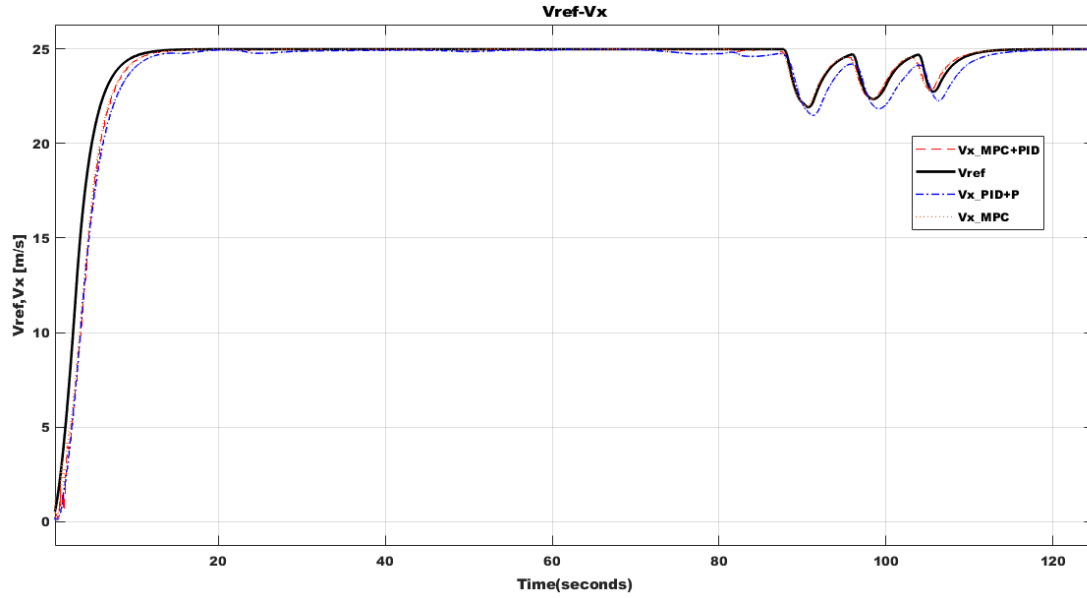


Figure 4.9: Measured vehicle's longitudinal speed V_x (dashed) vs. vehicle's longitudinal speed reference V_{ref} (solid)

coupled MPC controller and decoupled controller tracks speed profile better compared to decoupled controller MPC+PID and PID+P, but in decoupled controller the speed profile tracing is comes with cost of large variation in lateral deviation.

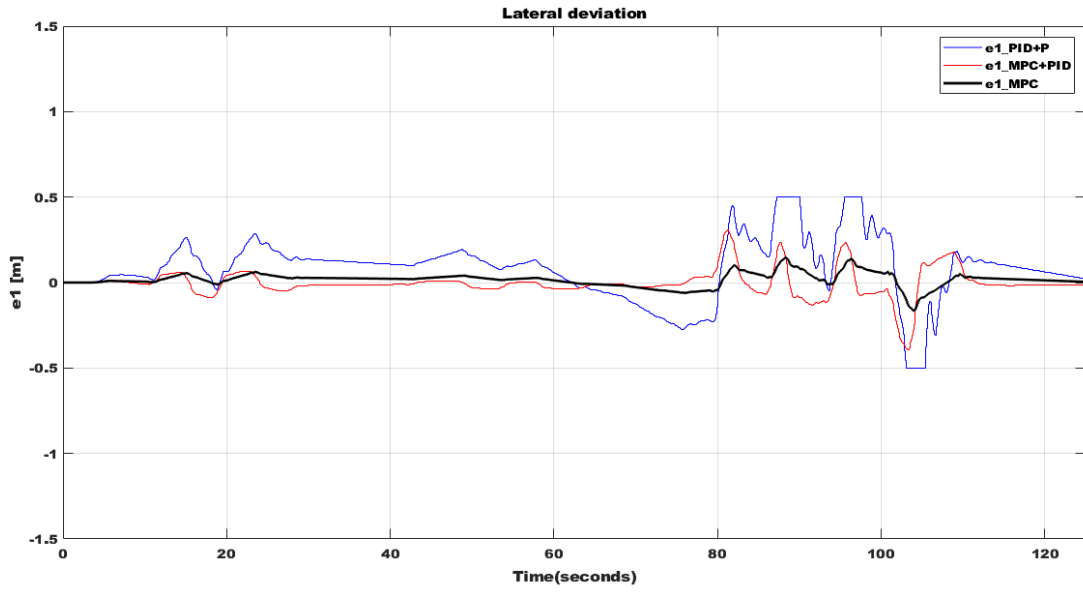


Figure 4.10: Lateral deviation e_1

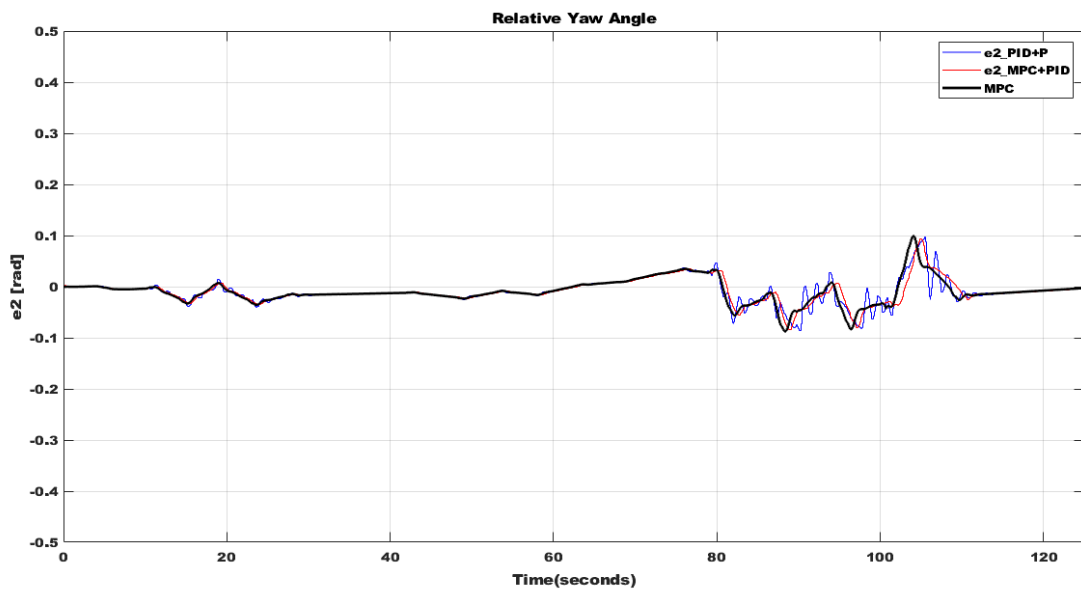


Figure 4.11: Relative yaw angle e_2

In coupled controller the lateral stability of the vehicle is maintained within limits. Maximum lateral deviation Figure 4.10 is 0.10m but for decoupled controller it reaches around 0.4m, and the relative yaw angle Figure 4.11 is within limit of ± 0.10 rad for both controller.

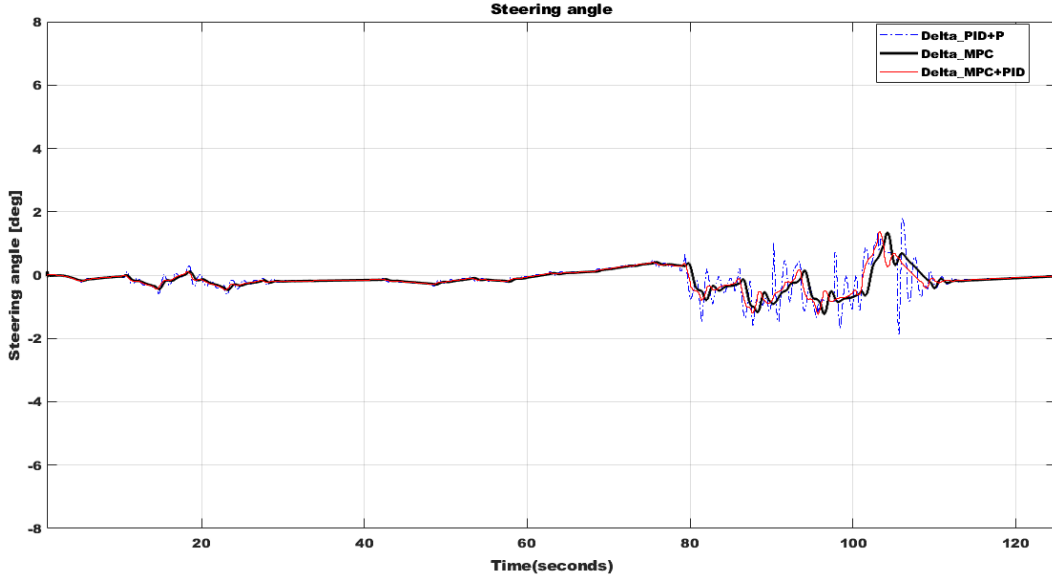


Figure 4.12: Front wheels steering angle command δ

From Figure 4.12, the steering angle is ± 1.5 degree in coupled controller. while in decoupled controller case, steering angle has higher frequency of oscillation and will cause the lot of jerk.

The lateral and longitudinal acceleration for three different controller are shown Figure 4.13-4.15. For MPC controller the longitudinal acceleration is 0.6g and lateral acceleration 0.9g, within the limit of driving condition. For MPC+PID and PID+P, the lateral acceleration is varying continuously due to oscillation in steering angle and longitudinal acceleration is around 0.5g.

Overall, the MPC controller perform quite well compare to decoupled one, by tracking the reference velocity accurately and keeping the errors, in terms of lateral deviation and relative yaw angle in the admissible limits. It also preserves the lateral stability of the vehicle and keeps the acceleration within the range.

4.3 Validation of Controller

The performance of the car on the racetrack is evaluated. Each dynamic tests different features of the vehicles. In addition to the maximum longitudinal and lateral acceleration, race performance, efficiency and endurance of the race car will be examined and evaluated. For this thesis, the Acceleration and Skid Pad are considered to evaluate the longitudinal and lateral acceleration.

4.3.1 Acceleration Test

The acceleration test evaluates the car's acceleration in a straight line on flat pavement. The vehicle's acceleration from a standing start is measured over a 75 metre straight. In addition to traction, the correct engine design is especially important, either in terms of greater power or for the highest possible torque. The accelera-

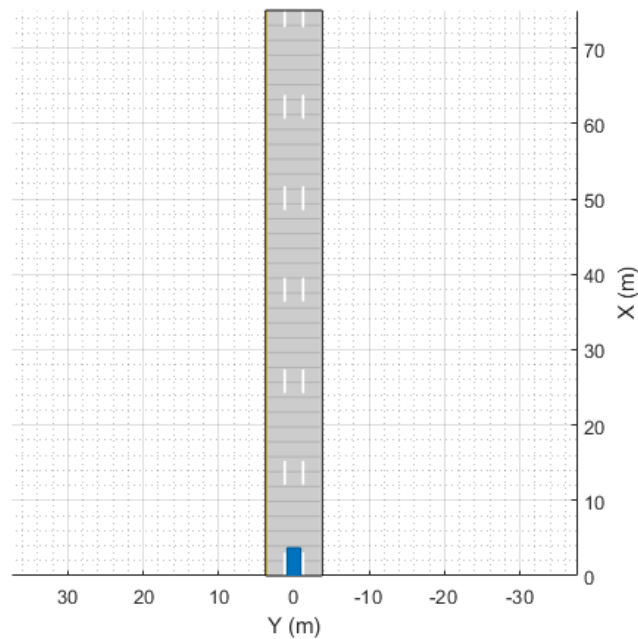


Figure 4.15: Acceleration Test Track

tion course length will be 75 m from starting line to finish line. The course will be at least 4.9 m wide as measured between the inner edges of the bases of the course edge cones. Cones are placed along the course edges at intervals of about 5

paces. As we see from Figure 4.17, the longitudinal acceleration is quite same for all

Controller	Maximum velocity (Kmph)	Time for maximum Velocity (s)	Longitudinal acceleration (m/s^2)	Longitudinal g's (g)
MPC	100	4.6	7.1	0.71
MPC_PID	100	4.7	7	0.70
PID_P	100	4.7	7	0.70

Figure 4.16: Acceleration Test Data

the controller, the controllers reaches 100 kmph within 4.6 seconds with maximum longitudinal acceleraiton is avout 0.7 g as shown in Figure 4.16

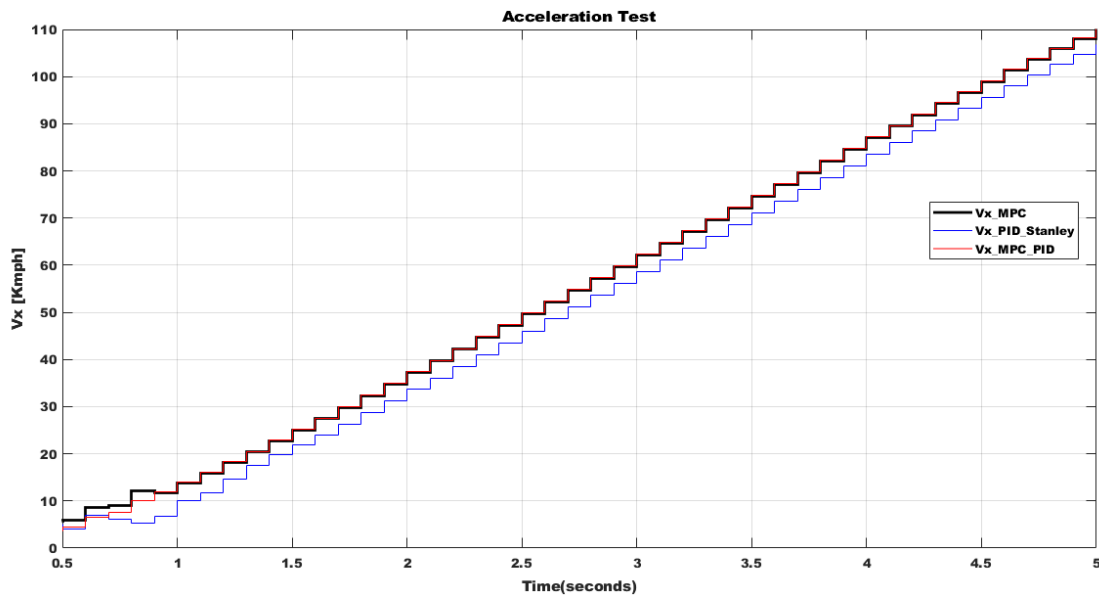


Figure 4.17: Logitudinal veocity

4.3.2 Skid Pad Test

The objective of the skid-pad test is to measure the racecar cornering ability on a flat surface while making a constant radius turn. During the Skid Pad test, the cars must drive a figure of 8 circuit lined with track cones, performing two laps of each circle. In each case, the second lap will be measured. The lap time gives a

comparative value for the maximum possible lateral acceleration of the car. Most of the cars use aerodynamics to raise the contact pressure and thus, increase lateral acceleration. There will be two pairs of concentric circles in a figure of eight pattern.

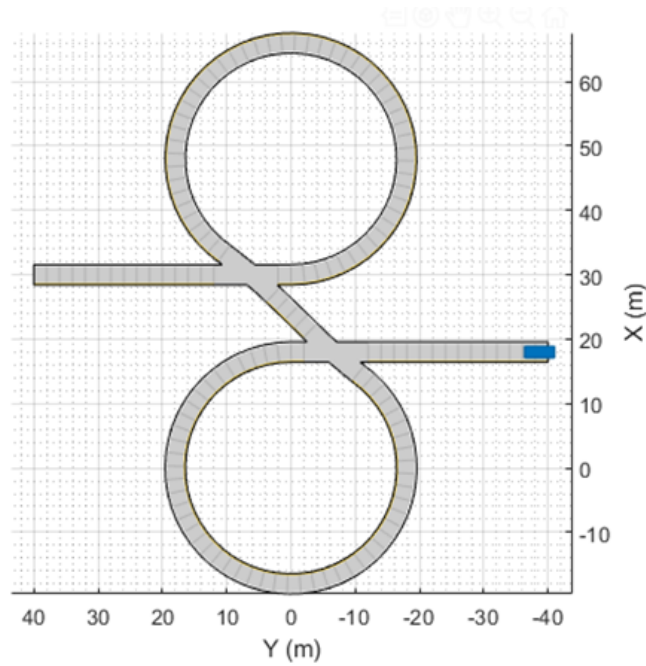


Figure 4.18: Skid-Pad Test Track

The centers of these circles will be 18.25 m apart. The inner circles will be 15.25 m in diameter, and the outer circles will be 21.25 m in diameter. The driving path will be the 3.0 m path between the inner and outer circles. The cars will enter and exit through gates on a 3.0 m wide path that is tangential to the circles where they meet. The lateral acceleration for three different controller are shown Figure 4.19.

Controller	Skid pad radius (m)	Velocity during cornering (kmph)	Lateral acceleration (m/s^2)	Lateral g's (g)
MPC	18	40	6	0.6
MPC_PID	18	34.5	5	0.5
PID_P	18	28	3.5	0.35

Figure 4.19: Skid-Pad Test Data

the maximum velocity was calculated from the equation 3.1 for a constant radius of curvature. MPC controller enters the track with maximum velocity of 40kmph and lateral acceleration 0.6g but in decoupled controller at 40kmph vehicle losses it control and enters into instability, for this speed is reduced to 34.5kmph and 25kmph for MPC PID and PID+P respectively with lateral acceleration about 0.5g and 0.3g.

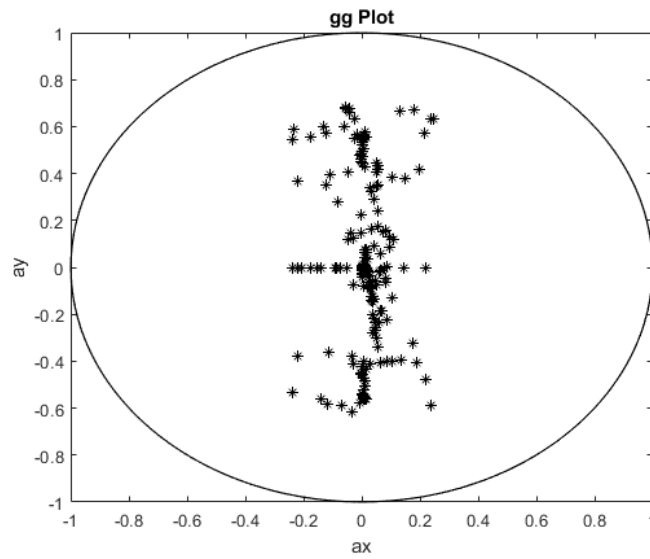


Figure 4.20: Skidpad MPC

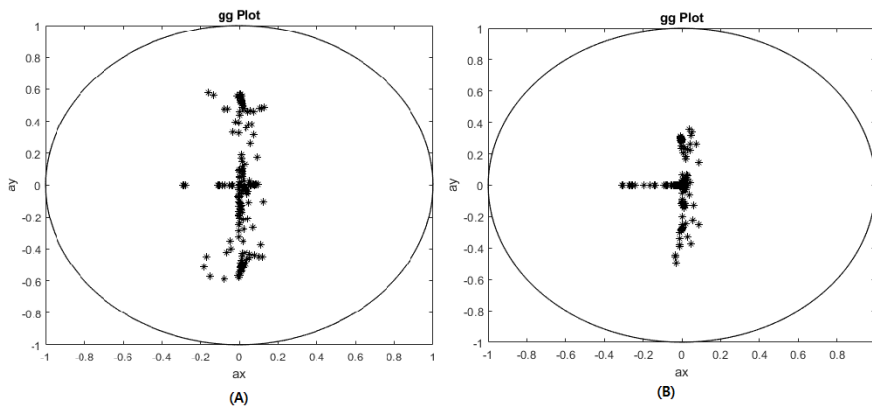


Figure 4.21: Skidpad (A)MPC+PID (B) PID+P

Chapter 5

Conclusions and future works

In this study, lateral and longitudinal control strategies for racing applications has been explored. A coupled model predictive controller is exploited, allowing to minimize the errors on the controlled variables, which are the lateral deviation, the relative yaw angle and the longitudinal speed of the vehicle w.r.t the reference longitudinal speed by acting on the steering angle of the front wheels and throttle/brake pedals, while driving the vehicle within the limits of adherence conditions. Three different control strategies have been tested through simulation on MATLAB and Simulink and MPC provides good performance for lateral guidance and accurately follows the reference speed profile. The lateral deviation was kept within the acceptable range of ± 0.1 m and also relative yaw angle was within the limit of ± 0.15 rad. Finally, it was compared to another controller based on MPC-PID and PID-Lateral control, which tackle the problem in decoupled way. From the results, it was seen that coupled MPC controller was able to control the car in a much better way and kept the lateral deviation and the relative yaw quite small compared to the other decoupled controller while maintaining the lateral stability of the vehicle.

In regards to future work, the focus will be on improvement of current work and development of system with new functions and technologies.

More precise tire model which yields higher control precision is essential. The coupled longitudinal and lateral tire forces with non-linearities can be considered.

Although assuming that friction coefficient is constant, the fact exists that friction coefficient changes slightly based on different road and weather conditions etc. Since friction coefficient is crucial for controlling of vehicle in both longitudinal and lateral planes, a function for friction coefficient estimation can be appended to control system.

Vehicle ride quality and handling performance can be improved through modification of vehicle dynamics in vertical directions and by integrating a suspension controller. Longitudinal dynamics can be modelled by adding driveline and tire forces with non-linearities to the prediction model. Also, actuator dynamics can be considered to make the controller more robust and to take into account the delays during actuation. Validation of 14 DOF Full Vehicle Model, should be tested in the simulations before testing on the actual model.

Some other future works can also be done to improve and extend this thesis work in the field of perception. First of all, in order to overcome the limitation of the lane detection function using the camera (crossroads or roads without lane marking), data coming from others sensors will be added, such as the data coming from a LiDAR and GPS. Making sensor fusion between camera and LiDAR, the detection will be improved in challenging scenarios. For the development of an autonomous racing vehicle.

To conclude, this thesis has contributed for autonomous vehicle research at Mechatronics Laboratory LIM (Laboratorio Interdisciplinare di Meccatronica) and the developed project can be used by future students to improve and continue the work in this interesting field.

Bibliography

- [1] Sperling D and D. Gordon, *Two Billion Cars: Driving Toward Sustainability*. Oxford University Press, 2009.
- [2] World Health Organization, *WHO Global status report on road safety 2018*. Weblink:https://www.who.int/violence_injury_prevention/road_safety_status/2018/en/.
- [3] Bryant Walker Smith, *Human error as a cause of vehicle crashes*. Weblink:<http://cyberlaw.stanford.edu/blog/2013/12/human-error-cause-vehicle-crashes>, December 2013.
- [4] Michele Bertonecello and Dominik Wee, *Ten ways autonomous driving could redefine the automotive world*. Weblink:<http://www.mckinsey.com>, June 2015.
- [5] Jennifer N Dang, *Statistical analysis of the effectiveness of electronic stability control (ESC) systems* Technical report, NHTSA, 2007.
- [6] M. B. K. Iagnemma, *Special issue on the darpa grand challenge, part 2*, Journal of Field Robotics, vol. 23, pp. 661–692, September 2006.
- [7] J. Funke, P. Theodosis, R. Hindiyeh, G. Stanek, K. Kritatakirana, C. Gerdes, D. Langer, M. Hernandez, B. Mller-Bessler, and B. Huhnke, *Up to the limits: Autonomous audi tts.*, in 2012 IEEE Intelligent Vehicles Symposium, pp. 541–547, June 2012.
- [8] A. Liniger, A. Domahidi, and M. Morari, *Optimization-Based Autonomous Racing of 1:43 Scale RC Cars*, Optimal Control Applications and Methods, vol. 36, p. 628 647, July 2014.
- [9] U. Rosolia, A. Carvalho, and F.Borrelli, *Autonomous racing using learning model predictive control*, ” American Control Conference (ACC), pp. 5115–5120, May 2017.
- [10] Dr.Ing.Peter Waldmann and Dipl. Ing. Daniel Niehues, *Der BMW Track*

- Trainer automatisiertes fahren im Grenzbereich auf der Nurburgring Nordschleife. Technical report* Tagung aktive Sicherheit, Lehrstuhl für Fahrzeugtechnik, Technical University of Munich, 2010.
- [11] Paul A Theodosis. *Path planning for an automated vehicle using professional racecar driving techniques*. PhD thesis, Stanford University, 2014.
- [12] Krisada Kritayakirana, *Autonomous vehicle control at the limits of handling*. PhD thesis, Stanford University, 2012.
- [13] Mike Hanlon. *Audi's autonomous Audi TT conquers Pikes Peak - how long before it betters a human driver?*
Weblink:<http://www.gizmag.com/audis-autonomous-audi-ttconquers-pikes-peak-how-long-before-it-betters-a-human-driver/17001/>.
November 2010.
- [14] Audi USA, *Piloted to the peak: Audi TTS Pikes Peak*.
Weblink:<http://www.audi.com/>, January 2016.
- [15] Je Cobb. *Driverless Audi RS7 blazes around Hockenheim circuit*
Weblink: <http://www.hybridcars.com/driverless-audi-rs7-blazes-around-hockenheimrace-circuit>. October 2014.
- [16] Steffen Muller, Michael Uchanski, and Karl Hedrick., *Estimation of the maximum tire-road friction coefficient*, Journal of Dynamic Systems, Measurement, and Control, 125(4):607, 617, 2003.
- [17] Alexander Liniger, Alexander Domahidi, and Manfred Morari, *Optimization-based autonomous racing of 1:43 scale RC cars*, Optimal Control Applications and Methods, 36(5):628–647, 2015.
- [18] Robin Verschueren, Stijn De Bruyne, Mario Zanon, Janick V. Frasch, and Moritz Diehl., *Towards time-optimal race car driving using nonlinear MPC in real-time*, In Proceedings of the IEEE Conference on Decision and Control, volume 2015-Febru, pages 2505–2510, 2014.
- [19] Tamás Keviczky, Paolo Falcone, Francesco Borrelli, Jahan Asgari, and Davor Hrovat, *Predictive control approach to autonomous vehicle steering*, American Control Conference, pages 4670–4675, 2006.
- [20] Florent Althé, Philip Polack, and Arnaud de La Fortelle, *A Simple Dynamic Model for Aggressive, Near-Limits Trajectory Planning*, IEEE IV 2017 conference, June 2017.

- [21] Jason Kong, Mark Pfeiffer, Georg Schildbach, and Francesco Borrelli, *Kinematic and Dynamic Vehicle Models for Autonomous Driving Control Design*, pages 2–7, July 2015.
- [22] F Borrelli, P Falcone, T Keviczky, J Asgari, and D Hrovat., *MPC-based approach to active steering for autonomous vehicle systems*, International Journal of Vehicle Autonomous Systems, 3(2/3/4):265, 2005.
- [23] Krisada Kritayakirana and J. Christian Gerdes, *Autonomous vehicle control at the limits of handling*, International Journal of Vehicle Autonomous Systems, 10(4):271–296, 2012.
- [24] Jarrod M Snider, *Automatic Steering Methods for Autonomous Automobile Path Tracking*, Work, (February):1–78, 2009.
- [25] Mogens Graf Plessen, Pedro F. Lima, Jonas Martensson, Alberto Bemporad, and Bo Wahlberg, *Trajectory Planning Under Vehicle Dimension Constraints Using Sequential Linear Programming*, April 2017.
- [26] D. Fischer and R. Isermann. *Mechatronic semi-active and active vehicle suspensions*. Control Engineering Practice, vol. 12, no. 11, pp. 1353–1367, 2004
- [27] C. Ghike and T. Shim. *14 degree-of-freedom vehicle model for roll dynamics study*. SAE Technical Paper, Tech. Rep., 2006.
- [28] G. Venture, P.-J. Ripert, W. Khalil, M. Gautier, and P. Bodson. *Modeling and identification of passenger car dynamics using robotics formalism*. IEEE Transactions on Intelligent Transportation Systems, vol. 7, no. 3, pp. 349–359, 2006.
- [29] U. Kiencke and C. Nielsen. *Automotive Control Systems* Springer-Verlag, 2000.
- [30] D. Wang and F. Qi. *Trajectory planning for a four wheel steering vehicle*. IEEE International Conference on Robotics and Automation, Seoul, Korea, May 21-26, 2001.
- [31] MATLAB [Online]. *Vehicle Body 3DOF*. 2018.
Weblink:<https://it.mathworks.com/help/vdynblks/ref/vehiclebody3dof.html>.
- [32] Rajamani R. *Vehicle Dynamics and Control*, Mechanical Engineering Series, 2012.
- [33] Rachid Attia, Rodolfo Orjuela, Michel Basset. *Combined longitudinal and lateral control for automated vehicle guidance*. Francis, 2014, 52 (2), pp.261-279. <10.1080/00423114.2013.874563>. <hal-01027591>

-
- [34] Paolo Falcone , H. Eric Tseng , Francesco Borrelli , Jahan Asgari, Davor Hrovat. *MPC-based yaw and lateral stabilisation via active front steering and braking*. 46:S1, 611-628, DOI: 10.1080/00423110802018297
- [35] J. G. Fernandez. *A Vehicle Dynamics Model for Driving Simulators*. Master's Thesis, Chalmers University of Technology, 2012
- [36] M. Short, M.J. Pont and Q. Huang. *Simulation of Vehicle Longitudinal Dynamics*. Technical Report ESL 04-01, 2004
- [37] Pacejka, Hans B. (2006). *Tyre and vehicle dynamics* (2nd ed.). SAE International. pp. back cover.
- [38] F. Borrelli, P. Falcone, T. Keviczky, J. Asgari and D. Hrovat. *MPC-Based Approach to Active Steering for Autonomous Vehicle Systems, 2005*
- [39] T. D. Gillespie. *Fundamentals of Vehicle Dynamics* Michigan, USA: SAE International, Feb. 1992. [Online]. Available: <http://books.sae.org/book-r-114ntrl>
- [40] R. Stone and J. K. Ball, *Automotive Engineering Fundamentals* Warrendale, Pa: SAE International, 2004. [Online]. Available: <http://books.sae.org/book-r-199>.
- [41] SAEJ670e Society of Automotive Engineers 1976, *Vehicle Dynamics Terminology*, "[Online]. Available: <http://standards.sae.org/j670> 200801/
- [42] J. Kang, R.Y. Hindiyeh, S. Moon, J.C. Gerdes, K. Yi. *Design and Testing of a Controller for Autonomous Vehicle Path Tracking Using GPS/INS Sensors* Proceedings of the 17th World Congress The International Federation of Automatic Control Seoul, Korea, July 6-11, 2008
- [43] R. T. O'Brien, P. A. Iglesias, and T. J. Urban. *Vehicle Lateral Control for Automated Highway Systems* IEEE Transactions on Control Systems Technology, Vol. 4, No. 3, 1996.
- [44] MATLAB [Online]. *Visual Perception Using Monocular Camera*. 2018. Weblink:<https://it.mathworks.com/help/driving/examples/visual-perception-using-monocular-camera.html>.
- [45] J. W. Rutter. *Geometry of Curves*. Chapman & Hall/CRC, 2000.
- [46] Xu, Jin, et al. *An experimental study on lateral acceleration of cars in different environments in Sichuan, Southwest China*. Discrete Dynamics in nature and Society 2015.
- [47] J. Richalet, A. Rault, J. Testud and J. Papon. *Model predictive heuristic*

- control: Applications to industrial processes*. Automatica, vol. 14, no. 5, pp. 413–428, 1978.
- [48] C. Cutler and B. Ramaker. *Dynamic Matrix Control - A Computer Control Algorithm*. Automatic Control Conference, San Francisco, CA, 1980.
- [49] S. J. Qin and T. A. Badgwell. *A Survey of Industrial Model Predictive Control Technology*. Control Eng. Practice, 11, 733, 2003.
- [50] F. Borrelli, A. Bemporad and M. Morari *Predictive Control for linear and hybrid systems*. Cambridge University Press, Cambridge In preparation, 2015
- [51] D. E. Seborg, D. A. Mellichamp, T. F. Edgar, F. J. Doyle. *Process Dynamics and Control*. John Wiley and Sons, 2011.
- [52] F. Holzmann, B. Chrétien, H. Zeng, T. Gallner, and G. Spiegelberg *Integrated longitudinal and lateral controls on drive-by-wire platform to improve the road safety*. In SAE Technical Paper. SAE International, 04 2008.
- [53] R. Attia, R. Orjuela, and M. Basset. *Combined longitudinal and lateral control for automated vehicle guidance*. Vehicle System Dynamics, 52(2):261–279, 2014.
- [54] G. M. Hoffmann, C. J. Tomlin, M. Montemerlo, and S. Thrun. *Autonomous automobile trajectory tracking for off road driving: Controller design, experimental validation and racing* in 2007 American Control Conference, July 2007, pp. 2296-2301.